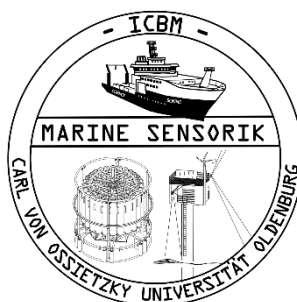


Spatial and temporal patterns of NO_3^- in an island beach ecosystem utilizing UV photometry

Coralie Lässig



Spatial and temporal patterns of NO₃- in an island beach ecosystem utilizing UV photometry

Bachelor thesis

Coralie Lässig

Coastal and marine management

Major marine biology

LKZ428VNAO1

Student ID 000008815

Advisors

Tjibbe Stelwagen & Peter Smit

Patrick Bron (Opponent)

Van Hall Larenstein

Leeuwarden, Netherlands

Prof. Dr. Oliver Zielinski

Kai Schwalfenberg

Institute for Chemistry and Biology of the Marine Environment (ICBM)

University of Oldenburg, Germany

Oldenburg, Germany

July 2019

All rights reserved

Acknowledgements

After four months full of field work on Spiekeroog, lab work and meetings with my advisors in Leeuwarden and Wilhelmshaven as well as long days and nights at my desk writing this work, my bachelor thesis of the study Coastal and Marine Management at Van Hall Larenstein is finally ready to be read. However, this work would not be possible without the people who supported me in such a great way during the process and who I want to thank here.

First of all, I would like to thank my advisors at Van Hall Larenstein and at the ICBM:

Tjibbe Stelwagen and Peter Smit - my advisors at Van Hall Larenstein – For the great commitment to give me extensive and helpful feedback on my work, I really appreciated this a lot.

Kai Schwalfenberg - my advisor at the ICBM– for the help during the preparation of the field experiments and during the field work, as well as the great support even at 5 A.M. collecting sensors from the cold North Sea. But also for the helpful technical know-how and for giving me constructive feedback on my work.

Prof. Dr. Oliver Zielinski - my advisor at the ICBM– for providing me the possibility to write my bachelor thesis at the ICBM, taking me into his working group (Marine Sensor Systems) and entrusting me such an interesting project for my bachelor thesis.

Furthermore, I would like to thank Daniela Meier for the great help with MATLAB and during field work on Spiekeroog, all people involved in the BIME sampling campaign in March 2019 and the whole ICBM and especially the working group Marine Sensor Systems for letting me use the institute's equipment and facilities.

I would also like to thank the staff at TriOS GmbH for providing me equipment, but also for teaching me about photometry previous to this thesis project. A special thanks goes to the technical support team of TriOS: Anni, Sven and Yvonne for their kind help regarding equipment specific questions, but also to Rüdiger Heuermann for providing me the possibility to do this project.

Finally, I would like to thank my family and friends for always supporting me and for distracting me from my work when it was highly needed.

I hope you will enjoy reading my thesis,

Coralie Lässig

July 3, 2019, Oldenburg, Germany

Abstract

Spatial and temporal patterns in submarine groundwater discharge (SGD) of nitrate in a high-energy sandy beach system on Spiekeroog Island were examined utilizing UV photometry. SGD as pathway of nitrate was studied to gain better understanding of the variability of nitrate discharge and the factors causing this complexity in order to improve coastal management of eutrophication and assessment of nitrate fluxes. Spatial patterns were examined by collecting 72 pore water samples at four different shore heights along nine cross-shore transects covering sampling depths of 50 and 100cm and measuring nitrate concentration ex situ. Temporal patterns were studied by deploying a UV spectrometer in a filter tube in 80cm depth at the high water line and measuring nitrate in situ across four full tidal cycles. Quantitative analyses revealed diffuse, but highly variable patterns in the longshore direction, whereas distinct patterns were found in the cross-shore direction and across tidal cycles. Nitrate concentrations increased with shore height, which is likely a result of higher oxygen concentrations causing nitrification of ammonium into nitrate. Patterns across tidal cycles showed nitrate peaks shortly before high tide, a decline during high water and rising levels during low tide, likely resulting from mixing of sea water and pore water during high water, influences of salinity and a possibly time-delayed water exchange in the filter tubes. However, the relatively low nitrate concentrations found in the sandy beach system during this study support the findings of previous research suggesting a minor impact of SGD from the sandy beaches on Spiekeroog compared to SGD from the backbarrier tidal flats on total budgets of nitrogenous compounds entering the Southern North Sea. However, in other systems, where tidal flats are absent and impacts of nutrient pollution are higher, SGD fluxes of nitrate from sandy beaches play likely a more important role.

Content

1. Introduction	7
2. Methodology.....	11
2.1. Study site.....	11
2.2. Sampling design	12
2.2.1. Spatial patterns	13
2.2.2. Temporal patterns	15
2.2.3. Control variables	17
2.3. Sensor calibration and data preparation	17
2.4. Data analysis – Spatial patterns	18
2.4.1. Longshore patterns	18
2.4.2. Depth-dependent patterns	18
2.4.3. Cross-shore patterns.....	18
2.4.4. Control variables	18
2.5. Data analysis - Temporal patterns	19
2.5.1. Control variables	19
3. Results - Spatial patterns	20
3.1. Longshore patterns.....	20
3.2. Depth-dependent patterns.....	21
3.3. Cross shore patterns	22
3.4. Control variables	25
4. Results - Temporal patterns.....	26
4.1. Control variables	28
5. Discussion.....	29
5. 1. Temporal patterns	29
5.1.1. Limitations.....	30
5.2. Spatial patterns.....	30
5.2.1 Cross-shore patterns.....	30
5.2.2. Longshore patterns	31
5.2.3. Depth-dependent patterns	31
5.2.4. Limitations.....	31
6. Conclusion.....	33
References	34

Appendix I	I
Measuring principles of the spectral sensor OPUS.....	I
Appendix II	II
Equipment.....	II
Appendix III	III
Model assumptions – Spatial patterns	III
Control variables – Spatial patterns.....	IV
Appendix IV	V
Model assumptions – Temporal patterns.....	V
Control variables – Temporal patterns	VI
Appendix V	XI
GPS coordinates	XI
Appendix VI	XIII
Summary of excluded samples	XIII

1. Introduction

As one of the main limiting factors of primary production, nitrogenous compounds are crucial for life on earth and can be found in different forms in the atmosphere, soil and water (Kaiser *et al.*, 2011). The conversion into bioavailable compounds (such as nitrate and ammonium) is controlled by chemical, physical and biological factors (Herbert, 1999). Organisms use nitrogenous compounds to build up biomass as well as to gain energy during metabolic activities and finally release the by-products into the environment (Kaiser *et al.*, 2011). Consequently, the availability of nitrogenous compounds strongly affects biomass and diversity of ecosystems. Nitrogenous compounds occur naturally in systems and availability is controlled by natural processes, such as atmospheric deposition, decomposition, geological formations and lightning. However, anthropogenic activities, such as the production of waste in the agricultural sector and the use of these by-products as fertiliser, runoffs as well as waste from other industries and municipalities have the potential to increase the amounts of nitrogenous compounds in a system dramatically (Buss *et al.*, 2005). Increased levels of nitrogenous compounds stimulate eutrophication and have serious consequences, such as algal blooms and oxygen depletion (O'Neil *et al.*, 2012). Thus, eutrophication presents a serious threat to vulnerable ecosystems and has the potential to alter food webs, support opportunistic as well as fast reproducing species and even trigger regime shifts (OSPAR, 2010).

During the past decades, high nitrate availability was observed in the southern North Sea, which is an important habitat and foraging ground for various species (Common Wadden Sea Secretariat, 2016). However, in some areas of the Southern North Sea (such as Schleswig Holstein, Germany), a reduced probability of eutrophication has been recognized in recent years. Whereas in other areas, such as the Lower Saxon part the risk of eutrophication remains high and green macro algae coverage still exceeds background values (van Beusekom *et al.*, 2018). Apart from this, oxygen depletion, leading to high mortality rates of bivalves, polychaetes and meiofauna was observed in the Lower Saxon part of the Wadden Sea as a result of high nutrient availability (Kolbe *et al.*, 1995).

Implications of increased nitrate availability is a known problem and several reports regarding the environmental state of the southern North Sea addressed the problem and identified the German coastal zone as a hotspot for eutrophication: 'The national report on the eutrophication status of the German coastal region identifies the entire inner German Bight including the Wadden Sea as a problem area with regard to eutrophication' (Keppner *et al.*, 2012). Whilst the OSPAR Quality Status Report of 2010 identified eutrophication as a major threat to the German Lower Saxon part of the North Sea due to constant high nitrate levels (Keppner *et al.*, 2012). The seriousness of increased nitrate concentration is underlined by the European Union's legal actions against Germany due to the exceedance of critical values (European Commission, 2016). The treaty forces Germany to take stronger actions with regard to the prevention, reduction and monitoring of nitrate induced pollution (European Commission, 2018a) and highlights the importance of understanding mechanism which influence the occurrence of eutrophic states.

A factor, strongly influencing the trophic state of coastal waters, is the transport of terrestrial compounds into marine systems. High proportions of nitrogenous compounds in coastal waters have a land based origin and consequently, land-sea pathways highly affect the nitrate availability in marine systems (Andersen *et al.*, 2007). Nitrate is mainly transported by three mechanisms into marine systems: Riverine discharge, atmospheric deposition and submarine groundwater discharge (SGD) (Tamborski *et al.*, 2017). SGD is defined by Burnett *et al.* (2003) 'as any and all flow of water on continental margins from the seabed to the coastal ocean, regardless of fluid composition or driving force' (figure 1) and is globally observed (Moore, 1996).

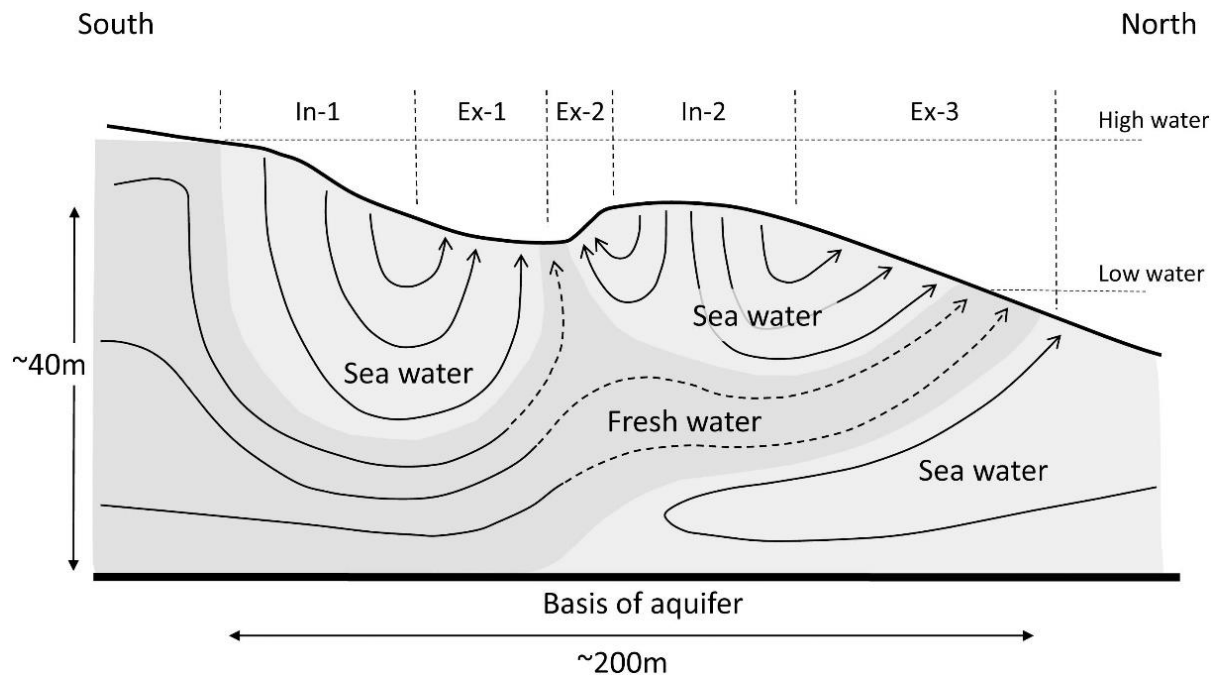


Figure 1. Schematic overview of SGD, illustrating the infiltration (In) and exfiltration (Ex) of fresh water and sea water at the Northern beach of Spiekeroog (Waska *et al.* 2019b).

The occurrence and impact of SGD depends on multiple factors: sandy sediment texture stimulates pore water seepage due to its permeable characteristics (Beusen *et al.*, 2013). Furthermore, the position of nearby aquifers, the tidal level and beach morphology affect the occurrence, intensity and spatial variability (regarding the longshore and cross shore direction, as well as depth level) of SGD (Lecher & Mackey, 2018) (Beck *et al.*, 2017). Apart from this, the occurrence of underground fresh water lenses effect the formation of SGD. On islands, where fresh water lenses are usually formed as a result of underground accumulations of fresh water, feed by precipitation and floating above denser sea water, SGD occurs and is more intense (Röper *et al.*, 2012). On small islands, where surface freshwater bodies are usually absent (Moosdorf *et al.*, 2015) SGD is from even greater importance due to the function as the main land-sea pathway for nutrient fluxes. As a result of the high variability of abiotic factors influencing pore water discharge, SGD is dynamic and often diffuse (Lee *et al.*, 2016). Strong temporal fluctuations across tidal cycles occur due to the variable steepness of the hydraulic gradient between pore and sea water levels (Billerbeck, 2005). These temporal and spatial variations complicate the analysis of SGD (Waska *et al.*, 2019a) (Burnett *et al.*, 2006) and therefore, a large proportion of previous studies did not consider the impact of temporal and spatial variability of SGD on nutrient transport. Especially in high energy systems, where stronger impact of waves, wind and tides increases the variability in SGD, assessing the magnitude of SGD on nutrient transport is even more complex (Waska *et al.*, 2019a).

Consequently, SGD, especially in high energy systems, is less studied than other nutrient transport mechanism (Burnett *et al.*, 2006; Kwon *et al.*, 2014) and for many years riverine discharge was believed to be the main input of terrestrial originated nitrate into marine systems and other factors were often neglected (Kwon *et al.*, 2014). However, several recent studies assume a significant effect of SGD on nutrient transport, which might even exceed the impact of riverine discharge in some areas (Waska *et al.*, 2019a; Cho *et al.*, 2018; Beck *et al.*, 2017; Kwon *et al.*, 2014; McCoy & Corbett, 2009), due to high volumes of pore water entering marine systems, the longer residence time of pore water in soils and the consequentially high nutrient concentration (Stalker *et al.*, 2009). Despite these indicators, SGD is not considered in current practices to manage and assess nutrient budgets entering marine systems: For example, the 'Wadden Sea Quality Status Report Eutrophication' stated a strong decline in riverine discharge of nitrate into the Wadden Sea since the early 1990's, but concluded that the growth potential of green macro algae did not decrease (van Beusekom *et al.*, 2018). However, the report considered riverine discharge as the only nutrient transport mechanism. The contradiction between decreasing riverine discharge and high algae growth potential leads to the assumption that other factors may play a key role in nutrient fluxes. At the moment no instruments in coastal and water management within Europe, such as the nitrates directives and the water framework directive consider SGD in assessing nutrient budgets and eutrophication. As stated by McCoy and Corbett (2009), neglecting SGD in management of coastal eutrophication is likely a result of the complexity and variability of SGD and its assessment, which results in an uncertainty regarding the magnitude and function of nitrate transport by SGD.

Therefore, the aim of this study was to contribute to better understanding of SGD in complex and less studied high energy beach systems and to reduce the uncertainty regarding the variability, function and magnitude of SGD as pathway of nitrate. Better understanding of SGD as nitrate transport mechanism might help to assess whether and how SGD as pathway of nitrate should be considered in coastal management. Consideration of SGD in the management of coastal eutrophication might improve the assessment and modelling of nutrient budgets entering marine systems and eventually reach one of the EU nitrate directive's aims of better monitoring of water quality regarding nitrate pollution (European Commission, 2018b). Specifically, better knowledge about spatial and temporal short term variability in nitrate discharge might contribute to improved monitoring and sampling strategies, which may result in qualitative as well as quantitative better data and more cost-effective monitoring practices and calculation of nutrient budgets. More accurate calculations of nutrient budgets might be the base for adjustments of existing regulations, such as the European fertilizer regulation or the nitrate directive.

Apart from this, the study aims to provide better understanding of the general function of SGD as land-sea pathway for nitrate. Since nitrate presents a main limiting factor of primary production, better knowledge about the variability of nitrate fluxes helps to understand and predict productivity in systems. Besides this, tide induced patterns in nitrate using optical in situ measuring techniques are not well studied and therefore, limited knowledge exists. Furthermore, the Wadden Sea system serves often as a model to understand mechanism which control tidal systems in general (Beck & Brumsack, 2012), understanding patterns of nitrate in the Wadden Sea area, might help to understand these mechanism in other areas as well.

Eventually, the outcomes of studies examining mechanism that control nutrient fluxes into marine systems are relevant to various parties, such as national and international authorities (e.g. the Minister for the Environment, Energy, Construction and Climate Protection of Lower Saxon, the German government, the European Commission), scientific institutions, but also the general public. Understanding the pathways of nitrate into marine systems helps to monitor pollution and identify vulnerable zones, which might help to designate water protection zones under the EU Water Framework Directive and help to conserve vulnerable ecosystems.

The bachelor thesis project 'Spatial and temporal patterns of NO_3^- in a beach ecosystem utilizing UV photometry' is integrated in the interdisciplinary campaign 'BIME' (barrier island mass effect). The working group Marine Sensory Systems of the Institute for Chemistry and Biology of the Marine Environment (ICBM) and the Institute of Biology and Environmental Sciences (IBU/University of Oldenburg) along with the Max Planck Institute for Marine Microbiology in Bremen cooperate in this campaign to study the barrier island mass effect of the East Frisian Islands focusing on Spiekeroog Island. Apart from this, the campaign aims to gain better understanding of the impact of submarine ground water discharge on mass transport of nutrients and trace metals as well as the composition and microbiology of pore water (Carl von Ossietzky Universität Oldenburg, 2018).

Research questions

From the described problem statement the following main research question emerged:

'What spatial and temporal patterns of nitrate transported by SGD occur in a sandy beach ecosystem?'

To examine this question the following sub questions were formulated:

Spatial patterns

- I. What variation in NO_3^- concentration can be observed in the longshore direction?*
- II. What difference in NO_3^- concentration can be observed between pore water samples collected at 500mm and 1000mm depth?*
- III. What variation in NO_3^- concentration can be observed in the cross-shore direction (HWL, runnel, ridge, LWL)?*

Temporal patterns

- I. What temporal variation in NO_3^- concentration can be observed across a tidal cycle?*

2. Methodology

2.1. Study site

Sampling was carried out on the East Frisian Island Spiekeroog located in the Southern North Sea (figure 2). Main parts of the island are designated as nature protection area (Röper *et al.*, 2013). Due to the island's barrier function differs the sediment structure between the exposed shore in the North and the sheltered backbarrier area in the South. In the North, where sampling took place, sand is the dominant sediment type, whereas in the South mainly muddy sediments are found (Dijkema, 1991). The absence of limnic water bodies suggests that SGD fed by an underlying water lens (Röper *et al.*, 2012) is the main fresh water input into the marine waters surrounding Spiekeroog. Spiekeroog was chosen as sampling location due to legal requirements, the occurrence of permeable and sandy sediment texture in the North, which stimulates pore water seepage (Beusen *et al.*, 2013) and the formation of a runnel system (Michel & Howa, 1999), the observation of pore water seepage in the past (Beck *et al.*, 2017), but also due to the availability of a research station on the island.

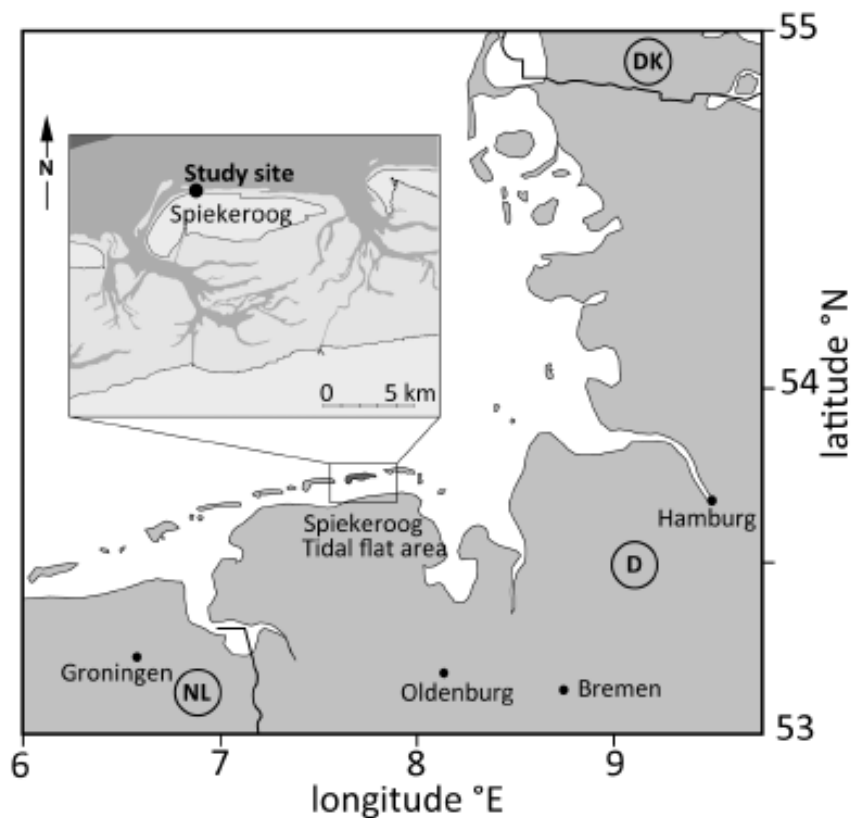
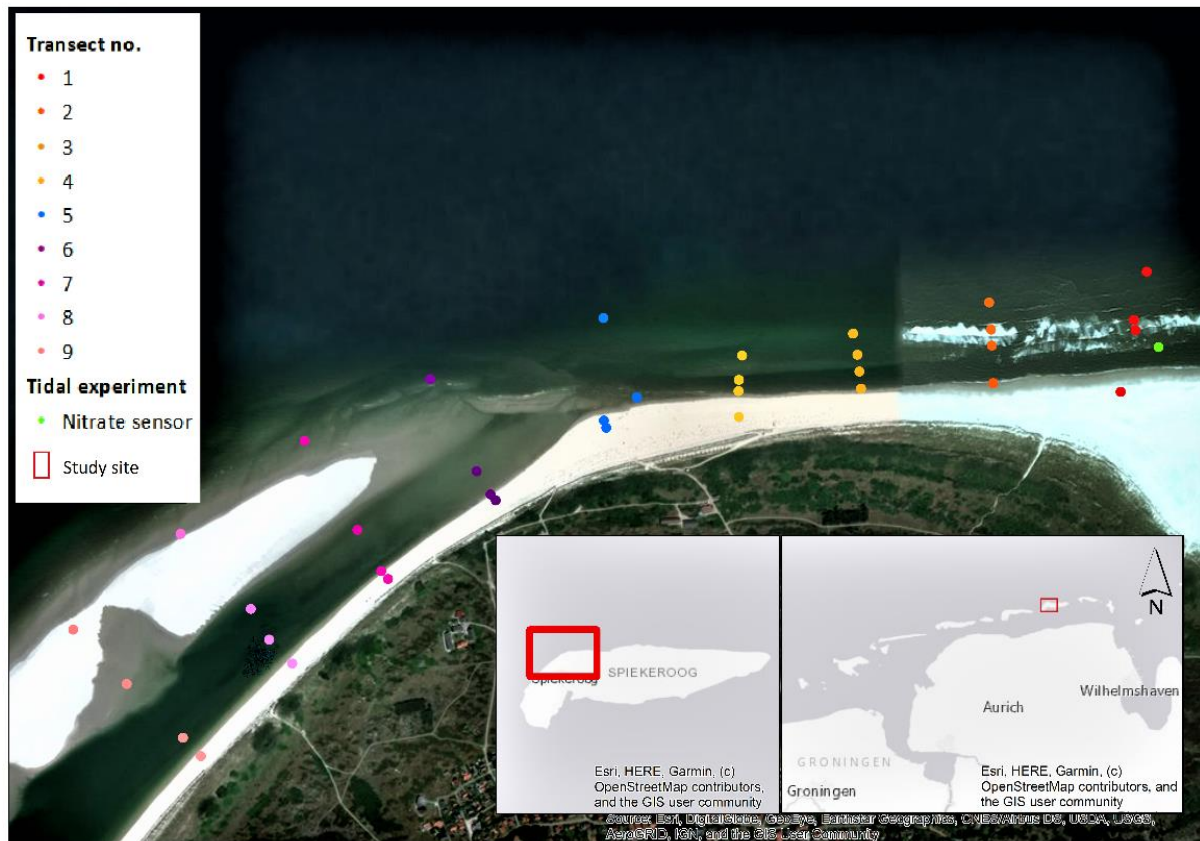


Figure 2. Map of the study area (Waska, *et al.*, 2019c).

2.2. Sampling design

To assess temporal and spatial patterns two different sampling strategies were applied. Spatial patterns were examined by collecting pore water samples from March 19 to 22, 2019 along nine transects (figure 3) and measuring samples ex situ. Whereas temporal patterns were studied by deploying nitrate sensors in the field (figure 3) and measuring nitrate in situ for 60 hours from May 14 to 17, 2019. In both approaches, nitrate was measured utilizing the UV spectral sensor OPUS by TriOS GmbH (Rastede, Germany) with a path length of 10mm.



Author: Coralie Lässig
Date: 25-June-2019
Coordinate system: WGS84 (zone 32 N)
Source basemap: Esri DigitalGlobe, GeoEye, Earthstar Geographic, CNES/Airbus DS, USDA, USGS, AeroGRID, IGN and the GIS user community

Figure 3. Map of the study area, showing the sampling points along the nine transects sampled to assess spatial patterns as well as the position of the in situ deployed nitrate sensors to examine temporal patterns.

2.2.1. Spatial patterns

To examine spatial patterns in nitrate discharge, nine vertical transects were sampled (figure 3). Distance between each transect was 300m and transect length was determined by the distance between MHWL and MLWL. The position of transects and sampling points was recorded using a high precision GNSS device (see appendix V). Along each transect, two pore water samples (from 50cm and from 100cm depth) were collected from each segment of the littoral zone (at the HWL, in the runnel, at the runnel ridge and at the LWL; see figure 5) which resulted in a sample size of eight samples per transect and a total sample size of 72 pore water samples. Samples were collected using a stainless steel pore water lance (figure 6) and filtered in the field using 0.7 μm ('Minisart NML GF non-sterile syringe filter' by Sartorius Stedim Biotech GmbH/Germany) and 0.2 μm ('Acrodisc 25mm' by Pall Corporation/USA) GRP filters. Samples were stored in the cold in sample-rinsed bottles and ex situ measured on the day of collection (to avoid changes in NO_3^- concentration over time) using a spectral nitrate sensors and a 10mm quartz cuvette. Each sample was ten times measured and the resulting mean nitrate concentration per sample was used in statistical analyses. 34 pore water samples were excluded from data analysis due to mean nitrate concentration under the detection limit ($< 1.0930 \mu\text{mol/L}$), which resulted in an actual sample size of 38 pore water samples. The majority of excluded samples was collected in the runnel (15 samples), followed by samples collected at the LWL (ten samples) and at the ridge (seven samples), whilst in no samples collected at the HWL nitrate concentration under the detection limit were found (see appendix VI). In addition eight sea water samples were collected as control group.

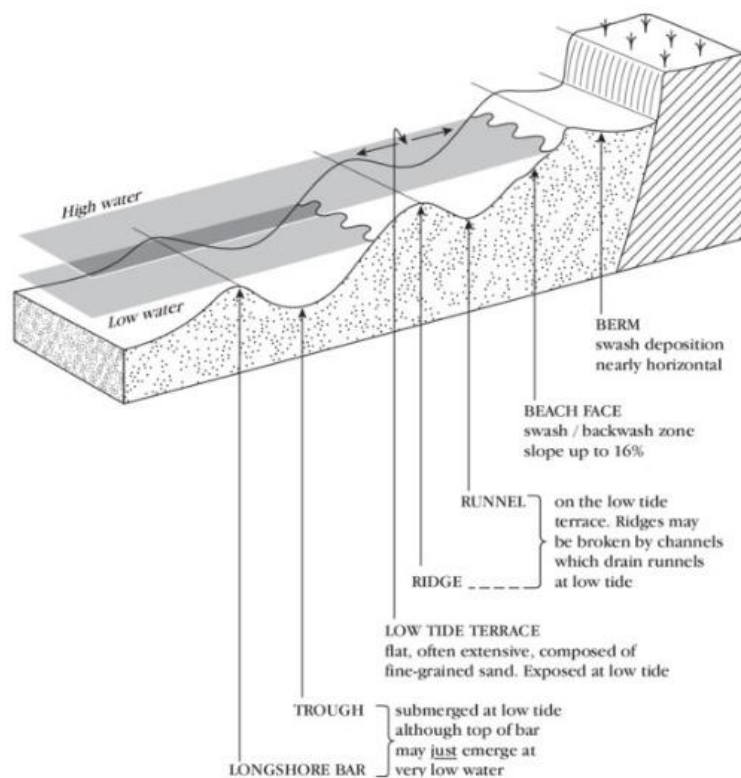


Figure 4. Schematic of the littoral zone showing the HTL, runnel, ridge and LWL (Bird et al., 2003).

Segments of the littoral zone

- HWL
- Runnel
- Ridge
- LWL



Figure 5. Cross shore segments of the littoral zone at the Northern beach on Spiekeroog Island.



Figure 6. Collecting pore water samples along the onshore transects using a pore water lance.

2.2.2. Temporal patterns

To study variations in nitrate discharge across tidal cycles, nitrate concentrations in pore water were measured in situ at the Northern beach (figure 3) using two spectral nitrate sensors. Prior to the actual experiment which was conducted from May 14 to 17, 2019, a pilot study has been carried out from March 26 to 29, 2019. During the actual experiment in May, the sensors were deployed in the sediment (in 80cm depth) at the MHWL and in a tidal runnel for 60 hours (figure 7). Runnel ridge systems are characterised by a longshore tidal stream, which is separated by a sandbar (runnel ridge) from the open sea during low tide and submerged during high tide. Since tidal runnels gather and channel the leaking pore water of an extensive area (Scott *et al.*, 2011) and no additional freshwater flux takes place from the ridge into the sea (Beck *et al.*, 2017), it is assumed that deploying sensors in the runnel enhances the measuring strategy. The positions of the sensors were recorded using a high precision GNSS device. Since OPUS sensors measure nitrate optically (appendix I) interference of particles needs to be avoided by hanging the sensors in closable HDPE filter tubes (filter width 0.3mm, tube length 1m, inner diameter 89mm; Figure 8 & 9) and protecting the optical path with a synthetic filter sleeve (filter width 0.3 μ m). To avoid darkening of the optical path by the filter sleeve, an aluminium grid sheet was placed between the optical path and the filter sleeve (see appendix II). CTD sensors were deployed in each tube to record the control variables conductivity and water temperature. The sensors were supplied with energy using a 14 V underwater rechargeable Li-Ion battery. Energy supply was controlled using a MicroDI Power Timer. The batteries' on time was programmed to 65 hours and the measuring interval of the optical and CTD sensors was set to 1 minute.

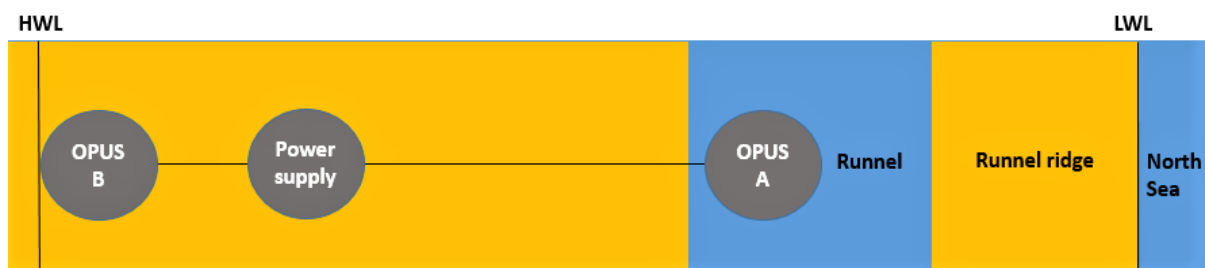


Figure 7. Schematic overview of the tidal experiment set up.

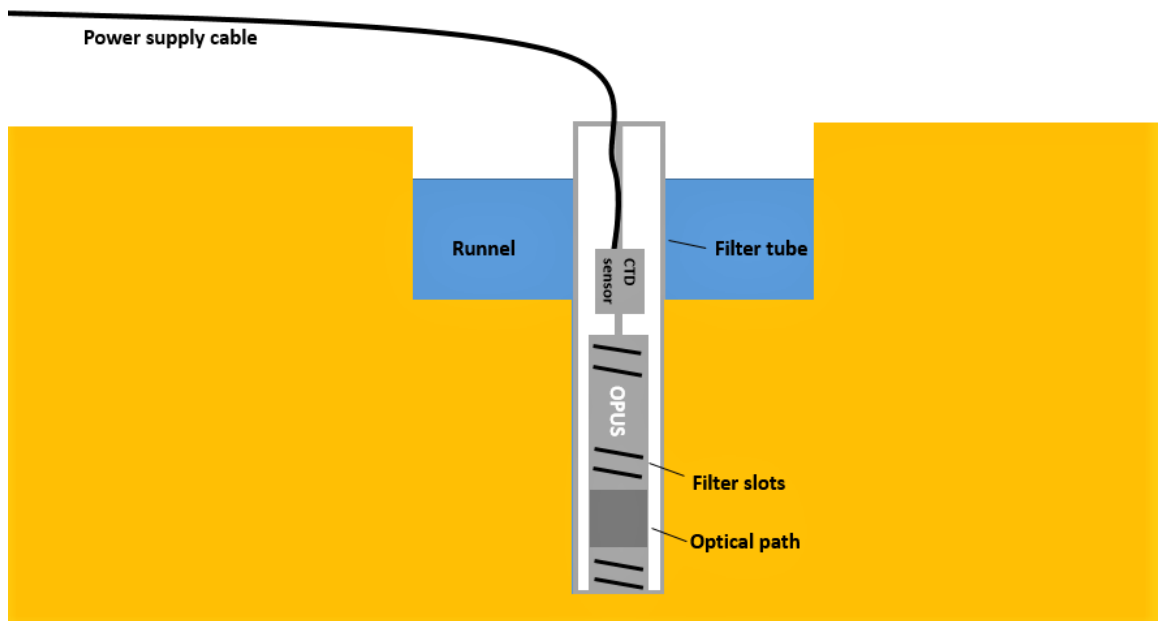


Figure 8. Schematic close up of the tidal experiment set up.



Figure 9. Deployment of the sensors and battery at the Northern beach on Spiekeroog.

2.2.3. Control variables

During transect sampling (spatial patterns), O₂ content [%], conductivity [mS/cm] and water temperature [°C] were recorded using a handheld multi meter. During the tidal experiment (temporal patterns), water temperature [°C] and conductivity [mS/cm] were measured in situ utilizing CTD sensors by vanEssen (measuring interval 1 min.). Conductivity and water temperature [°C] were measured to calculate the salinity in PSU. Since nitrate and bromide, which is a natural element present in sea water (Pinet, 2013) absorb at similar wavelengths of the UV spectrum (Pellerin *et al.*, 2013a) it is crucial to consider salinity in optical nitrate measurements and to take a possible distortion by bromide into account. Apart from salinity, the temperature influences the absorption spectrum of nitrate. Thus, strong temperature fluctuations might distort results and therefore, temperature needs to be considered (Pellerin *et al.*, 2013a). Since oxygen plays a key role in the nitrogen cycle and in the conversion of ammonium into bioavailable nitrate for primary producers (Campbell *et al.*, 2014), it is crucial to consider oxygen availability as well.

2.3. Sensor calibration and data preparation

Each nitrate sensor was specifically calibrated using ultra-pure water of type 1 with 0.055 µS/cm produced by an ultra-pure water system by Sartorius Stedim Biotech GmbH/Germany. Sensors for in situ deployment were calibrated in filter tubes, whereas sensors for ex situ application were calibrated using 10mm quartz cuvettes. Raw data was corrected using MATLAB 7.12 (The Math-Works Inc.) and a correction procedure developed by Zielinski *et al.* (2011). Temperature and salinity correction was performed by recording reference spectra of artificial sea water (low nutrient load; 12.5 PSU; 18 °C) and nitrate (16.13 µmol/L) in the lab. Reference spectra were then subtracted from the absorption spectra measured in the field. Eventually, nitrate was calculated by means of a linear regression between nitrate spectra of a dilution series conducted in the lab (2 to 100 µmol/L; increment 8 µmol/L) and the spectra measured in the field (Zielinski *et al.* 2011). Nitrate and salinity reference spectra were recorded prior to the field measurements in May. Therefore, salinity and nitrate ranges of the reference spectra were based on measured values during the pilot study in March.

2.4. Data analysis – Spatial patterns

Following data preparation, data was analysed using SPSS version 25 (IBM Corp, 2017). Results were considered statistically significant with $\alpha = 0.05$. GNSS data was processed using ArcMap version 10.5.1 (WGS84 32N; EPSG: 4326 projection) (Esri, 2016).

2.4.1. Longshore patterns

Longshore variability in nitrate concentration was examined for each segment of the littoral zone separately (HWL, runnel, ridge, LWL) due to high variability within transects. Since the variable nitrate concentration measured at each segment of the littoral zone did not satisfy model assumptions of a Pearson test (results of normality tests are shown in appendix III), a logarithmic transformation of the variable nitrate concentration was performed. Variability in nitrate discharge was then analysed by means of a Pearson correlation, which used the decadic logarithm of nitrate concentration as dependent variable and the transect number as independent variable.

2.4.2. Depth-dependent patterns

Since all samples collected in the runnel at 100cm depth were excluded from data analysis due to nitrate concentrations under the detection limit, no comparison regarding depth-dependent differences was conducted for these samples. Nitrate concentration per depth level met t-test's model assumptions regarding normality and variances, with exception of samples collected at the ridge in 100cm depth, which did not follow normal distribution (results of the tests are shown in appendix III). Therefore, nitrate concentration was logarithmically transformed. Depth depended variability in nitrate discharge was analysed by means of independent T-tests, which compared the decadic logarithm of nitrate concentration found in 50 cm and 100cm depth.

2.4.3. Cross-shore patterns

Differences in nitrate discharge in the cross shore direction were examined by comparing nitrate found at the different segments of the littoral zone (HWL, runnel, ridge, LWL). Since data did not satisfy model assumptions of an analysis of variances, a logarithmic transformation of the variable nitrate concentration was performed (results of the tests are shown in appendix III). Samples collected at the different segments of the littoral zone were compared by means of an analysis of variances (assuming unequal variances; results of the tests are shown in appendix III) and a Post Hoc comparison using a Games-Howell test (which considered the unequal variances and sample size).

Apart from this, cross shore trends in nitrate discharge were analysed by means of a Spearman correlation (since model assumptions of a Pearson correlation were not satisfied; the corresponding test results are shown in appendix III), which used the decadic logarithm of nitrate concentration as dependent variable and the shore height of the sampling point as independent variable.

2.4.4. Control variables

The relationships between nitrate concentration and the control variables were examined by means of Spearman correlations, since the variable nitrate concentration did not satisfy model assumptions of a Pearson correlation (test results are shown in appendix III). Therefore, Spearman correlations between nitrate concentration and salinity [PSU], between nitrate concentration and water temperature [°C] as well as between nitrate concentration and O₂ content [%] were performed. Apart from this, multicollinearity between the control variables was revealed, which indicated that model assumption of a multiple regression are not satisfied (see appendix III).

2.5. Data analysis - Temporal patterns

To examine temporal patterns of nitrate discharge across tidal cycles, 3651 nitrate measurements per nitrate sensor were conducted across 61 hours (measuring interval 1 min.). However, due to strong interference of very fine sediments causing reduced light availability, data quality was insufficient in measurements conducted in the tidal runnel. Therefore, only data measured at the HWL was considered in this study. The first 7 hours of measurements were excluded from data analysis (420 measurements) to avoid biased results caused by sensor deployment (e.g. low pore water levels in the filter tubes), which resulted in an actual sample size of 3231. Water level ranged from 21.797 to 345.791cm and nitrate concentration ranged from 8.9394 to 26.1098 $\mu\text{mol/L}$. Due to high variability in nitrate concentration between falling and rising tides, nitrate concentrations of both tidal intervals were analysed separately. The variable nitrate concentration did not satisfy model assumptions (test results are shown in appendix IV), however due to large sample size ($n = 3231$) the performance of parametric analyses was preferred. The relationship between water level and nitrate concentration was examined by means of a simple regression analysis, which used nitrate concentration as depended variable and water level as independent variable. Apart from this, differences in nitrate concentration during high and low tides were compared by means of an independent t-test, assuming normal distribution (test results of model assumptions are shown in appendix IV).

2.5.1. Control variables

A Pearson test was applied to test the correlation between nitrate and each control variable (salinity, water temperature). Apart from this, Pearson tests were performed to examine the correlation between water level and each control variable (salinity, water temperature). Although model assumptions of a Pearson test were not satisfied (test results are shown in appendix IV), the test was applied because of the sample size ($n = 3231$). Salinity ranged from 20.26 to 32.57 PSU ($\bar{x} = 29.6310$ PSU, $SD = 4.3701$), whilst water temperature ranged from 10.70 to 14.65°C ($\bar{x} = 12.0571$ °C, $SD = .71206$). Apart from this, a multicollinearity between the control variables was revealed (see appendix IV).

3. Results - Spatial patterns

3.1. Longshore patterns

No significant correlations between the decadic logarithm of nitrate concentration and the transect position were found at the HWL (Pearson, $r = 0.243$, $p = 0.347$), in the runnel (Pearson, $r = 0.409$, $p = 0.732$), at the ridge (Pearson, $r = 0.574$, $p = 0.065$) and at the LWL (Pearson, $r = 0.108$, $p = 0.818$). However, the data revealed high variability in nitrate concentration in the longshore direction as shown in table 1, figure 10 and 11.

Table 1. Nitrate concentration across the different transects and segments of the littoral zone.

Transect no	Segment littoral zone											
	HWL			Runnel			Ridge			LWL		
	N	\bar{x} NO ₃ - [$\mu\text{mol/L}$]	SD	N	\bar{x} NO ₃ - [$\mu\text{mol/L}$]	SD	N	\bar{x} NO ₃ - [$\mu\text{mol/L}$]	SD	N	\bar{x} NO ₃ - [$\mu\text{mol/L}$]	SD
1	2	48.693641	1.36805	1	3.7190*		2	6.085424	4.70091	1	1.4569*	
2	2	44.278221	2.1597		< detection limit			< detection limit			< detection limit	
3	2	57.192748	2.5798		< detection limit		2	19.5737	23.3353		< detection limit	
4	2	34.823912	5.13644		< detection limit			< detection limit			< detection limit	
5	2	41.5392	0.91389	1	1.9381*		1	22.7577*			< detection limit	
6	1	65.1411*		1	17.5424*		1	87.0602*		1	1.6898*	
7	2	57.905631	19.95		< detection limit		1	77.9050*		1	1.6436*	
8	2	63.827793	4.20655		< detection limit		2	35.221101	43.6754	2	1.525143	0.2217
9	2	44.43097	0.24312		< detection limit		2	45.579522	6.1823	1	3.2628*	

* single value

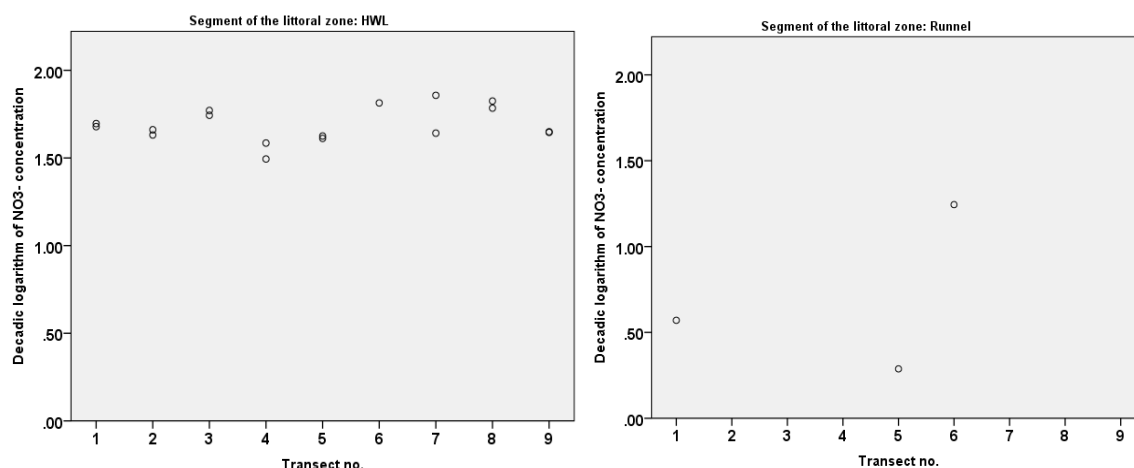


Figure 10. Variability in nitrate concentration across the onshore transects at the HWL and in the runnel.

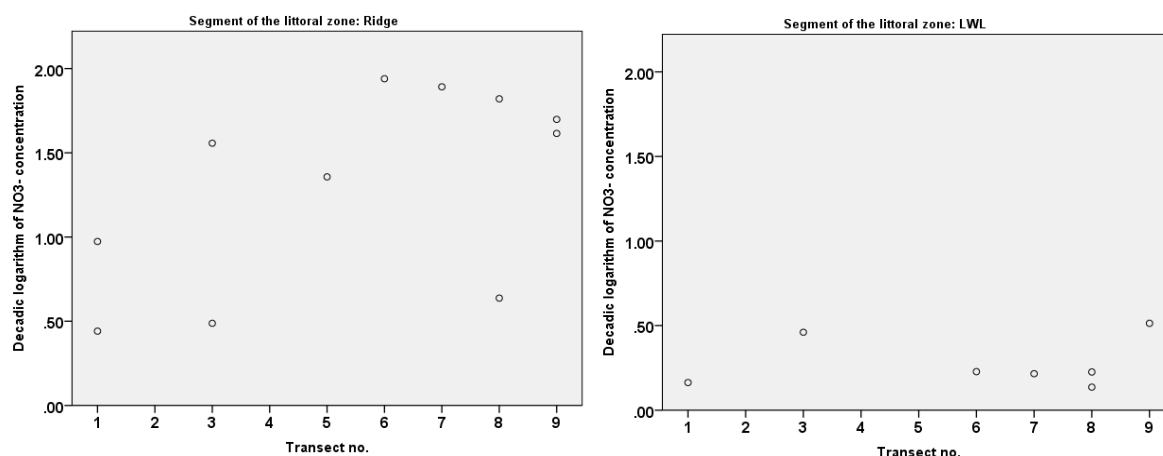


Figure 11. Variability in nitrate concentration across the onshore transects at the ridge and at the LWL.

3.2. Depth-dependent patterns

No significant differences between the decadic logarithm of nitrate found in pore water sampled in 50cm and 100cm depth were found at the HWL (Pearson, $r = 0.243$, $p = 0.347$), in the runnel (Pearson, $r = 0.409$, $p = 0.732$) and at the LWL (Pearson, $r = 0.108$, $p = 0.818$). In samples collected at the ridge, the mean decadic logarithm of nitrate found at 50cm depth was significant higher than in samples collected at 100cm depth ($t(9) = 2.804$, $p = 0.021$; Table 2; Figure12)

Table 2. Means of nitrate concentration and decadic logarithm found in pore water sampled at 50cm and 100cm depth.

Depth level [cm]	Segment littoral zone											
	HWL			Runnel			Ridge			LWL		
	N	\bar{x} NO ₃ - [$\mu\text{mol/L}$]	SD	N	\bar{x} NO ₃ - [$\mu\text{mol/L}$]	SD	N	\bar{x} NO ₃ - [$\mu\text{mol/L}$]	SD	N	\bar{x} NO ₃ - [$\mu\text{mol/L}$]	SD
50	8	46.0598	8.9644	3	7.73318	8.5416	7	48.6456	29.0391	3	2.0916	1.0236
100	9	53.5608	12.4005	< detection limit			4	15.0309	23.2901	4	1.9294	0.6487
	N	\bar{x} lg10	SD	N	\bar{x} lg10	SD	N	\bar{x} lg10	SD	N	\bar{x} lg10	SD
50	8	1.6559	0.0867	3	0.7006	0.4915	7	1.5935	0.3421	3	0.2885	0.2694
100	9	1.7185	0.1005				4	0.8161	0.5942	4	0.1989	0.131

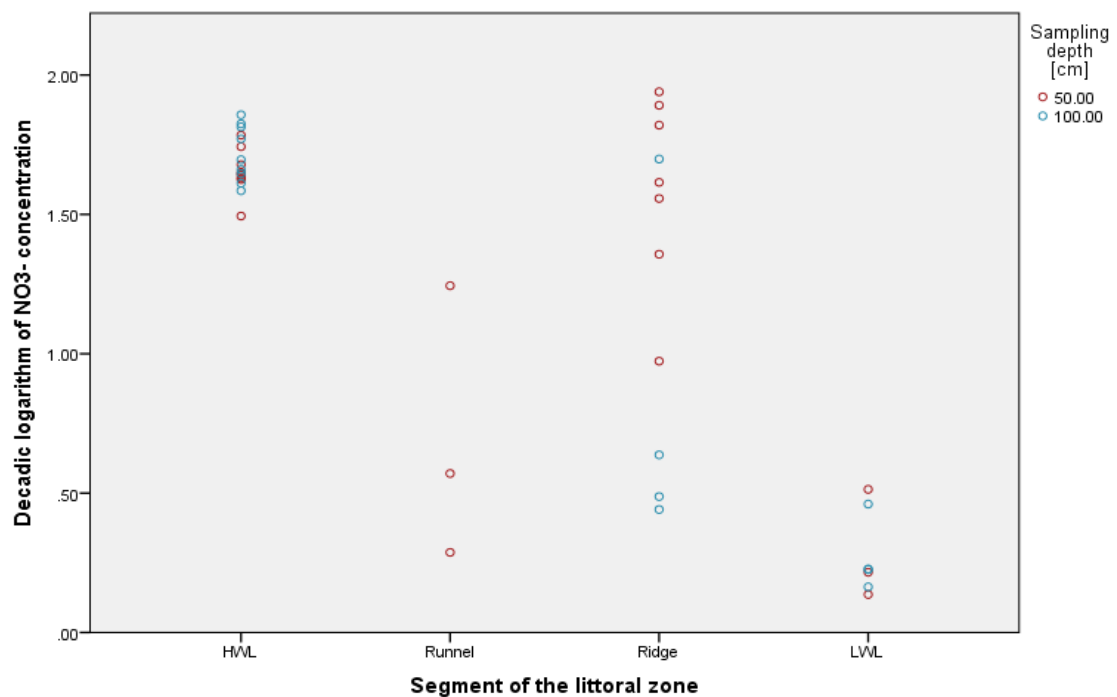


Figure 12. Distribution of the decadic logarithm of nitrate found in pore water sampled at 50cm and 100cm depth across the different segments of the littoral zone.

3.3. Cross shore patterns

An analysis of variances revealed significant differences in the mean decadic logarithm of nitrate concentration found in samples collected at the HWL, in the runnel, at the ridge, at the LWL and in sea water ($F(4, 41) = 10.917, p < 0.001$). Apart from this, a multiple Post Hoc comparison using a Games-Howell test indicated significant differences between the mean decadic logarithm of nitrate concentration found in samples collected at the HWL and LWL ($p < 0.001$), HWL and sea water ($p < 0.001$), LWL and sea water ($p < 0.001$) as well as between samples collected at the ridge and LWL ($p = 0.001$; see table 3 and figure 13 to 16).

Table 3. Nitrate concentration and the corresponding decadic logarithm found in pore water sampled at the different segments of the littoral zone.

Littoral zone	HWL	Runnel	Ridge	LWL	Sea water
N	17	3	11	7	8
\bar{x} NO ₃ ⁻ [μmol/L]	50.0309	7.733180	36.4220	1.9989	22.4988
SD NO ₃ ⁻	11.2667	8.5416	30.9243	0.7531	2.1778
\bar{x} lg10	1.6891	0.7006	1.3108	0.2776	1.3504
SD lg10	0.0968	0.49147	0.5744	0.1479	0.04191

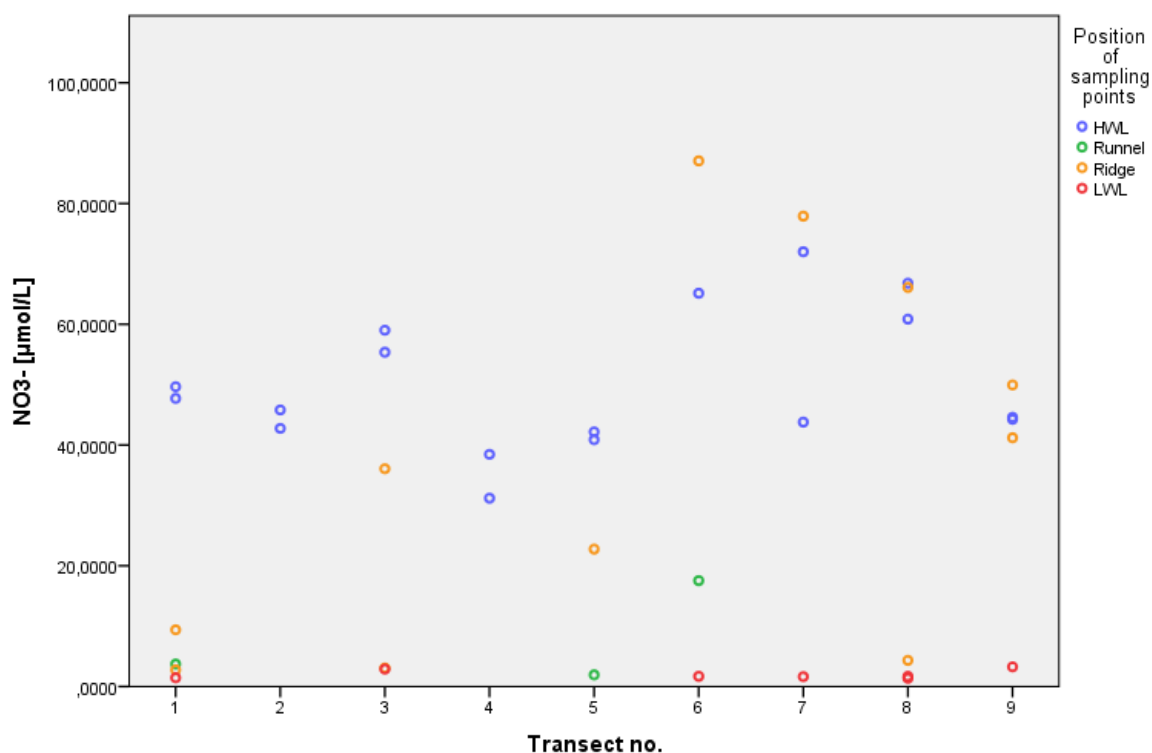
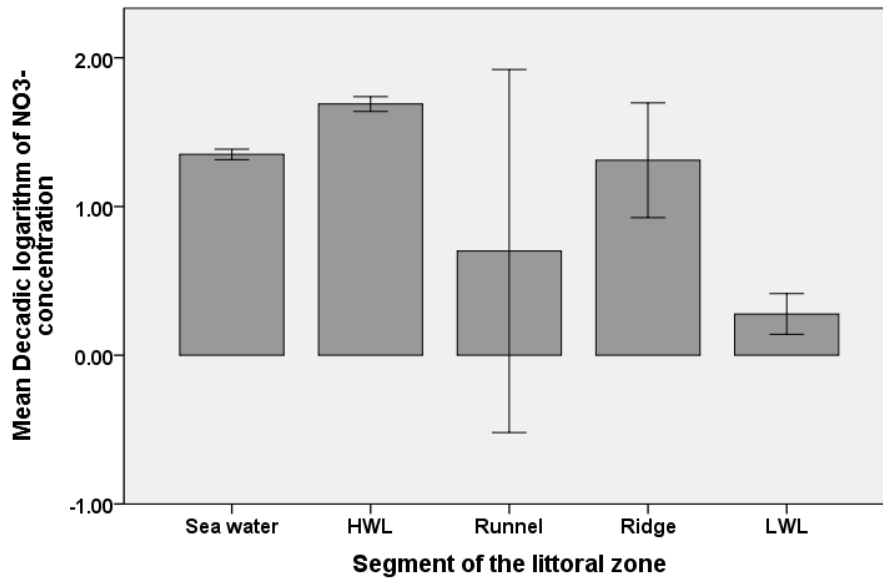


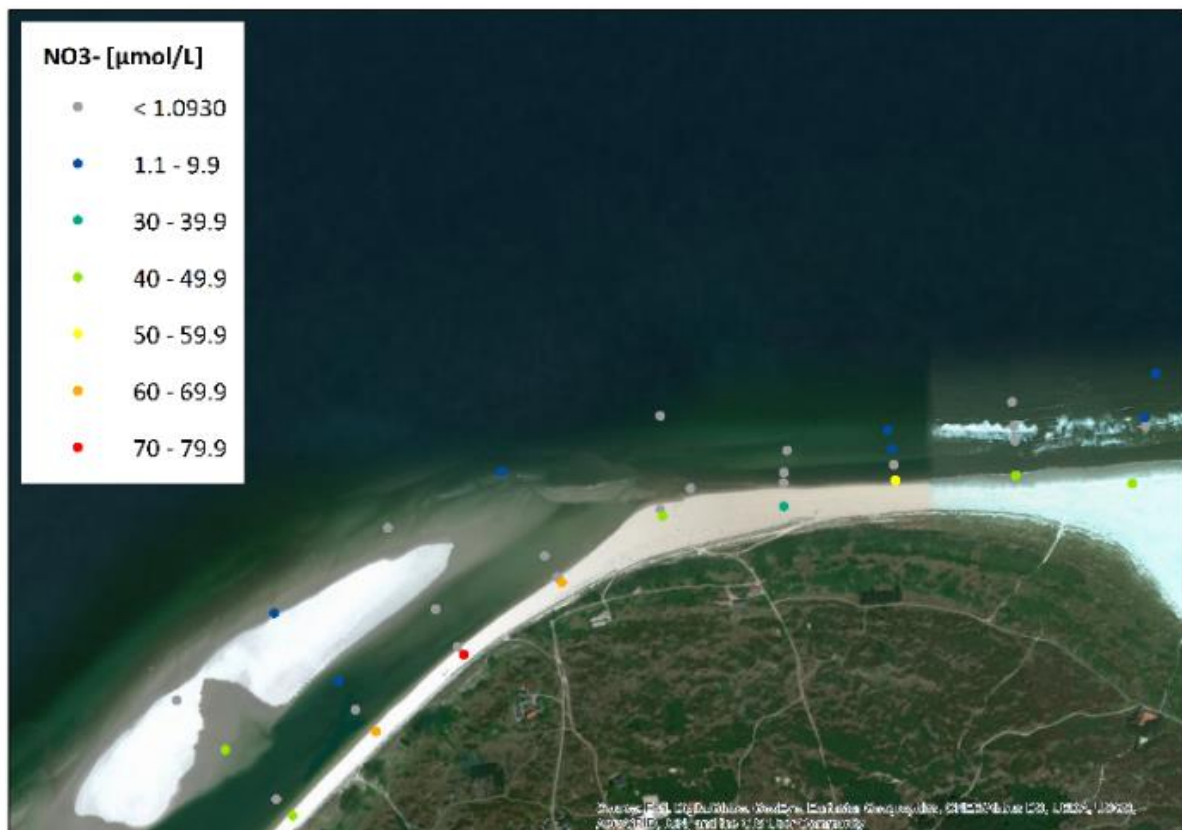
Figure 13. Variation in NO₃⁻ concentrations across the different segments of the littoral zone.



Error Bars: 95% CI

Figure 14. Differences in the mean decadic logarithm of nitrate concentration found in pore water samples collected at the HWL, in the runnel, at the ridge, at the LWL and offshore.

Spatial patterns in nitrate concentration found at 100cm depth



Author: Coralie Lässig

Date: 25-June-2019

Coordinate system: WGS84 (zone 32 N)

Source basemap: Esri DigitalGlobe, GeoEye, Earthstar Geographic, CNES/Airbus DS, USDA, USGS, AeroGRID, IGN and the GIS user community

0 0,5 1 Kilometers



Figure 15. Spatial patterns of nitrate discharge (100cm depth)

Spatial patterns in nitrate concentration found at 50cm depth

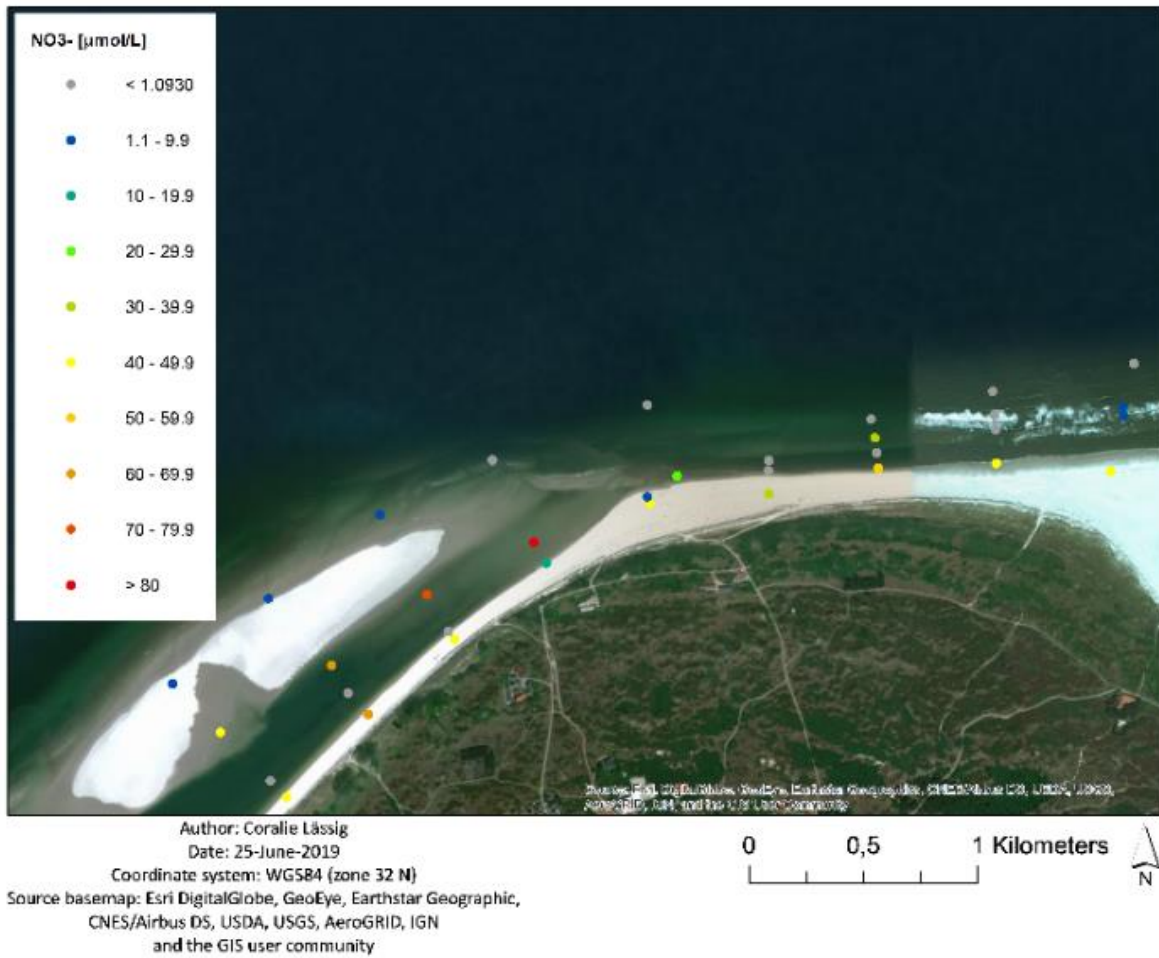


Figure 16. Spatial patterns of nitrate discharge (50cm depth).

Besides this, a significant positive correlation between the decadic logarithm of nitrate concentration and the shore height (sampling position at the littoral zone) was revealed (Spearman, $\rho = 0.626$, $p < 0.001$; Figure 17).

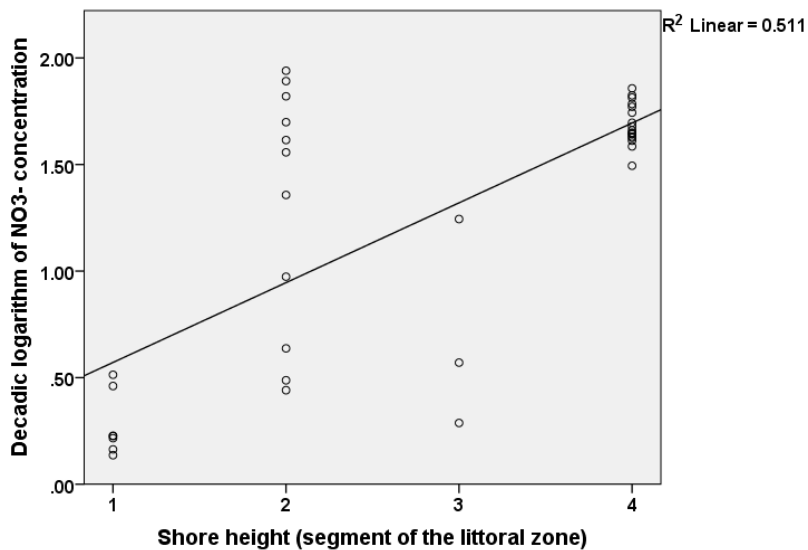


Figure 17. Positive correlation between the decadic logarithm of nitrate concentration and the shore height (position at the littoral zone; 1 = LWL, 2 = Ridge, 3 = Runnel, 4 = HWL).

3.4. Control variables

The relationship between nitrate concentrations in pore water samples ($n = 38$) and the control variables salinity, o₂ content and water temperature were analysed by means of a spearman correlation. The analyses indicate a negative correlation between nitrate concentration and salinity (Spearman; $\rho = -0.602$, $p < 0.001$; Figure 18) and a positive correlation between nitrate concentration and O₂ concentration (Spearman; $\rho = 0.682$, $p < 0.001$; Figure 19)

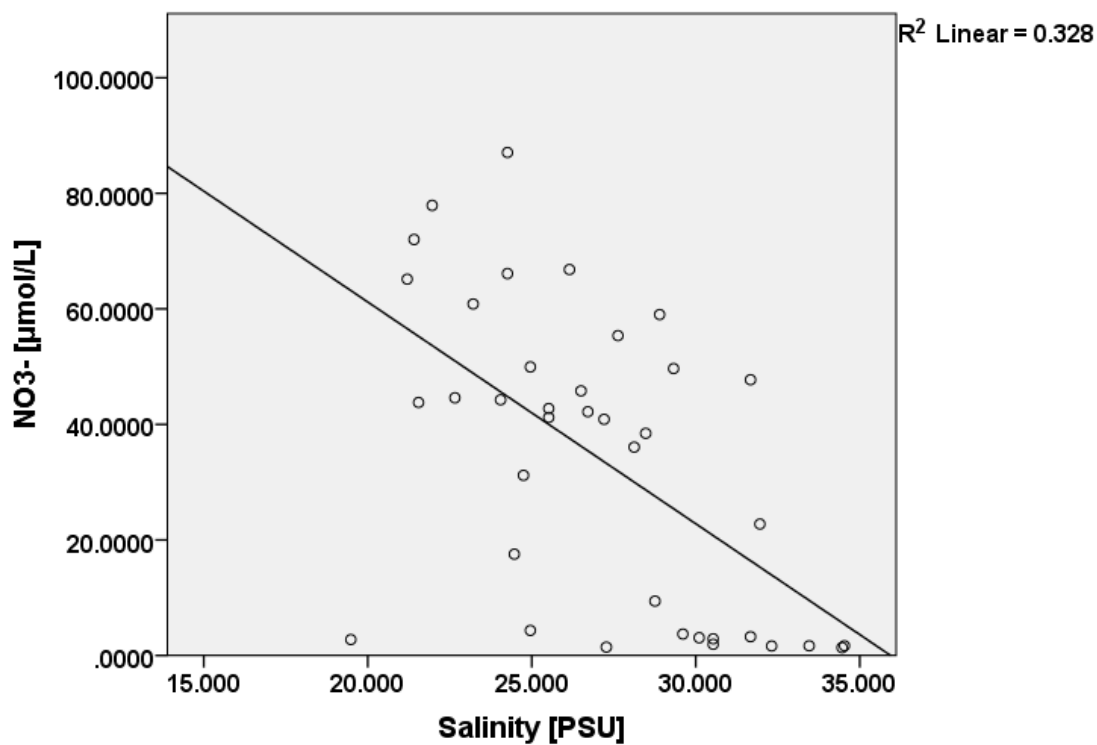


Figure 18. Negative correlation between nitrate concentration and salinity in pore water samples.

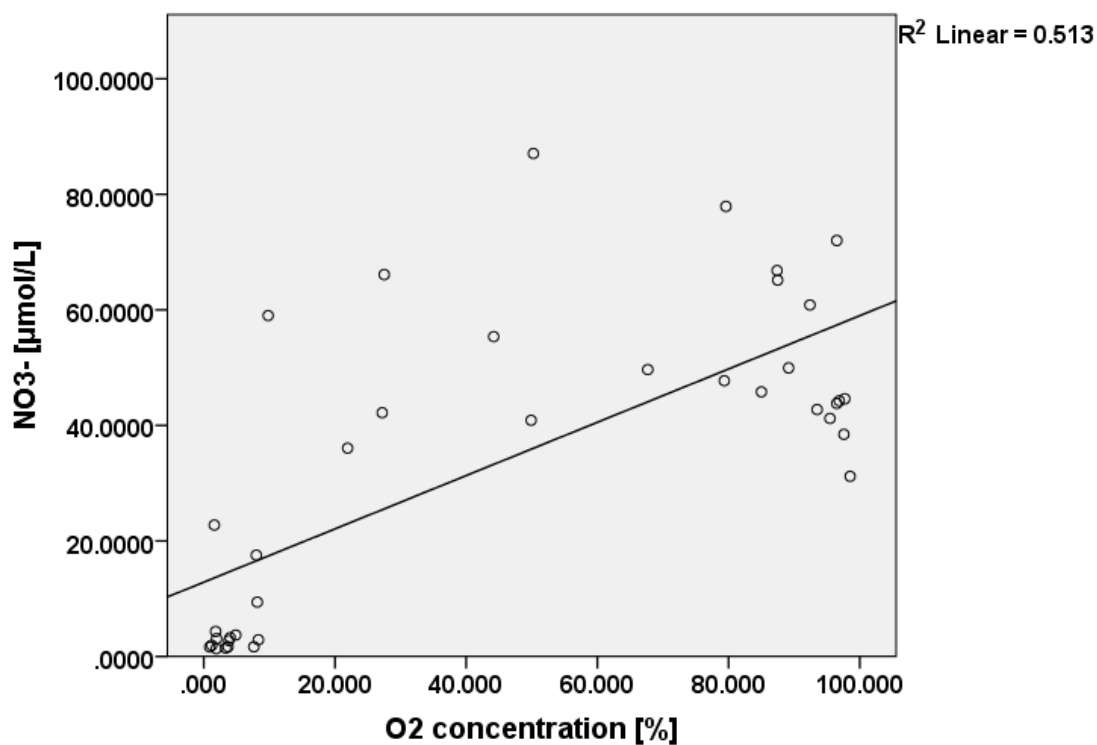


Figure 19. Positive correlation between nitrate concentration and O₂ content in pore water samples.

4. Results - Temporal patterns

The relationship between water level and nitrate concentration was examined by means of a simple regression analysis, which reveals a significant curvilinear correlation between nitrate concentration and water level during rising tides ($F(3, 1457) = 182.215, p < 0.001$) and falling tides ($F(3, 1766) = 267.607, p < 0.001$) as shown in figure 20 and 21.

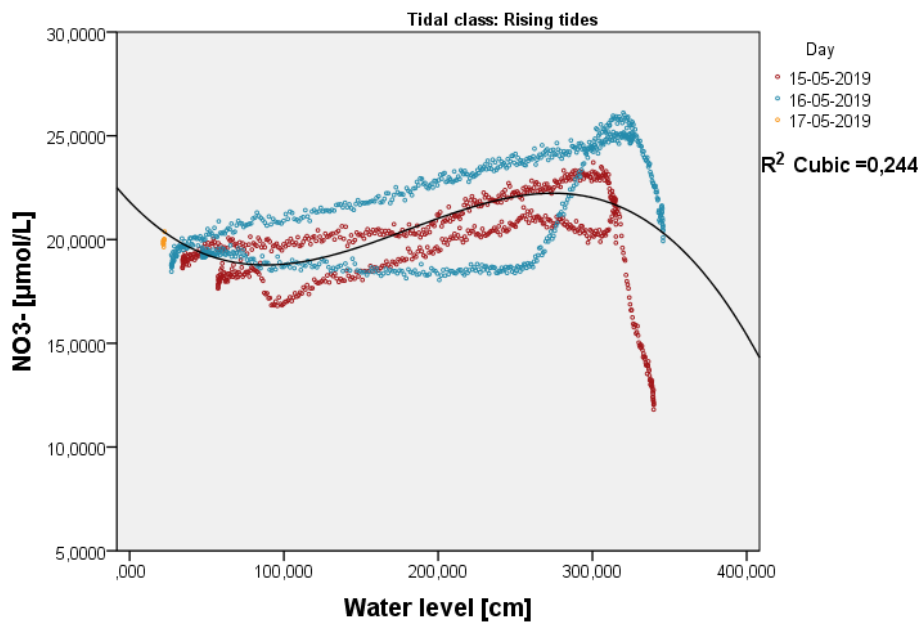


Figure 20. Curvilinear relationship between nitrate concentration and water level during rising tides.

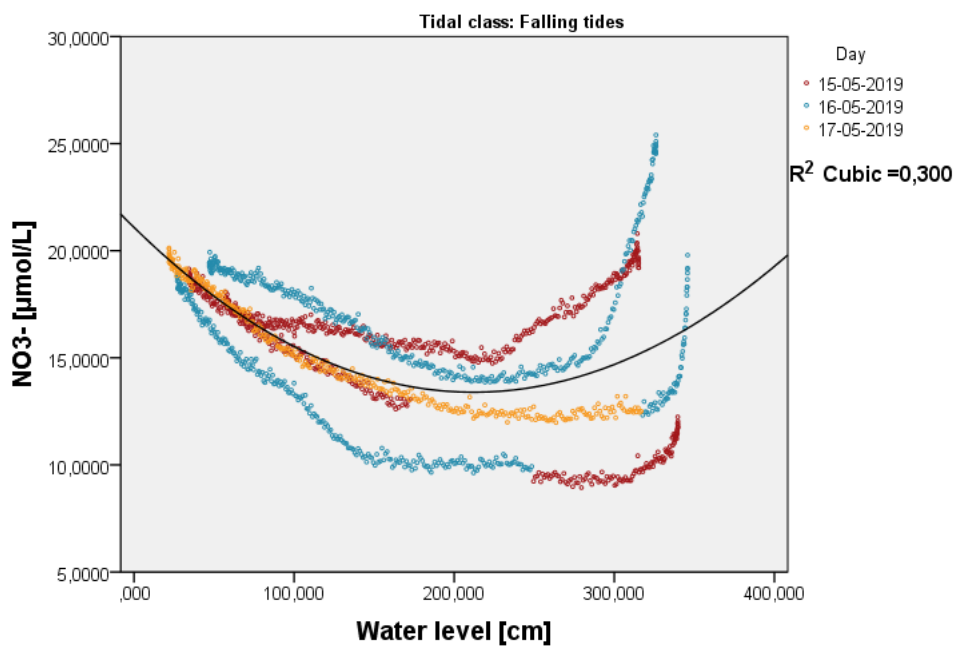


Figure 21. Curvilinear relationship between nitrate concentration and water level during falling tides.

Apart from the curvilinear correlation between nitrate concentration and water level, a distinct pattern regarding peaks and lows in nitrate concentration was observed across the tidal cycles (as shown in figure 22, 23 and 24). During rising tides, nitrate concentration increased until a tidal level of $\approx 15\text{cm}$ below the upcoming high tide level and then declined sharply during high tide resulting in nitrate concentrations of 12.0362 to $25.403 \mu\text{mol/L}$ ($n = 4$, $\bar{x} = 19.3021 \mu\text{mol/L}$, $SD = 5.4984$) during high water. During falling tides, nitrate concentrations declined further until a tidal level of ≈ 60 to 130cm below the previous high tide level (as shown in table 4). From this point on, nitrate concentration increased again until low tide, where nitrate concentrations of 17.7878 to $19.7940 \mu\text{mol/L}$ ($n = 4$, $\bar{x} = 18.8558 \mu\text{mol/L}$, $SD = 0.7427$) were observed. During and after low tide nitrate levels remained more stable but increased again until $\approx 25\text{cm}$ below the water level of the upcoming high water (peaks and lows in nitrate concentrations and the corresponding tidal levels are shown in appendix IV). A t-test comparing the mean nitrate level during high and low tide did not reveal significant differences ($t(7) = -0.183$, $p = 0.860$). However, as shown in table 4, nitrate concentrations during high tide indicated higher variability than during low tide.

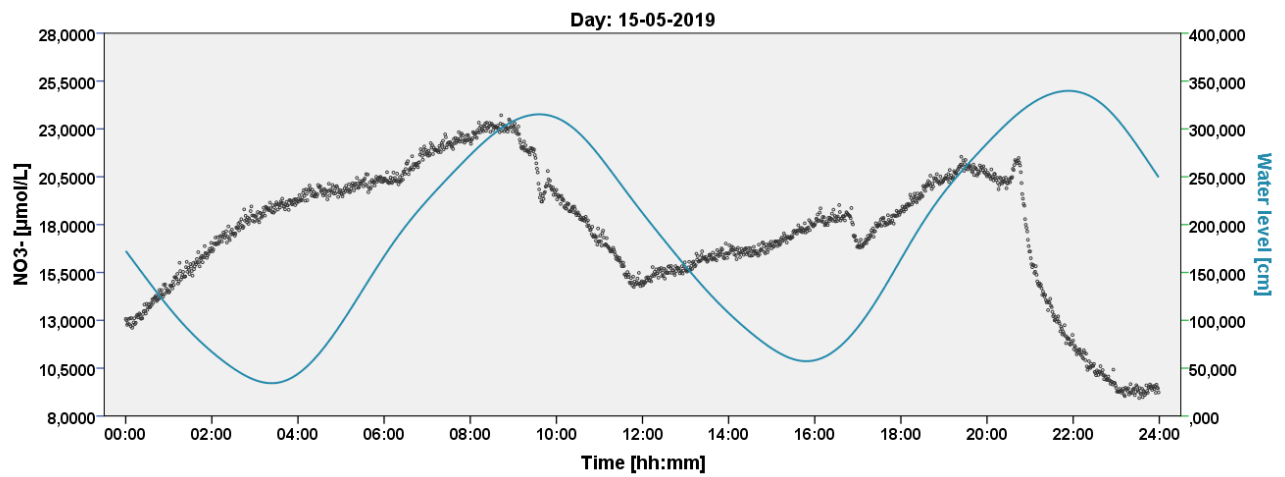


Figure 22. Variation in nitrate concentration across two tidal cycles measured on May 15th, 2019.

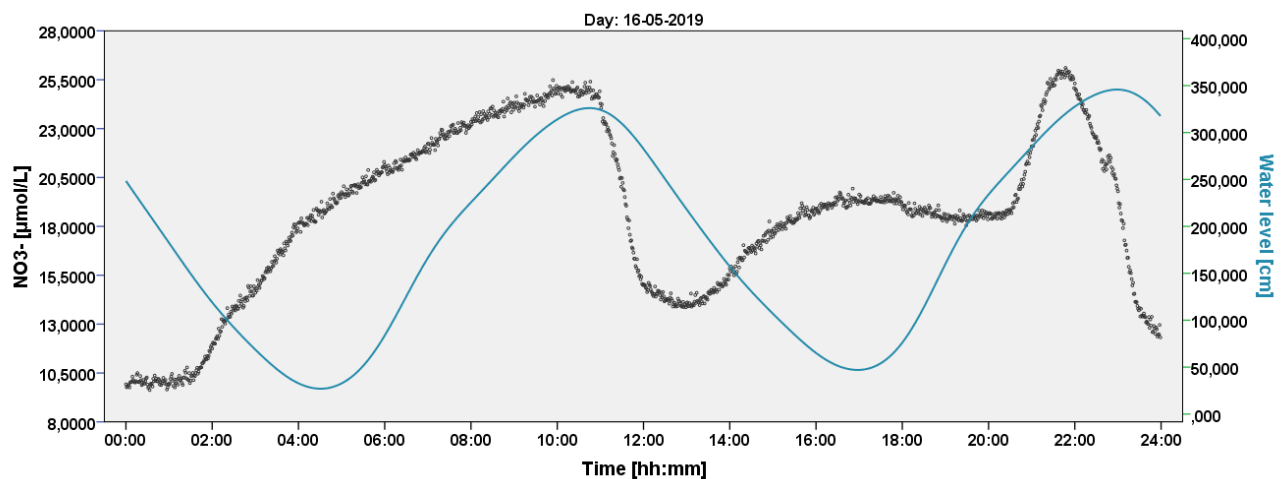


Figure 23. Variation in nitrate concentration across two tidal cycles measured on May 16th, 2019.

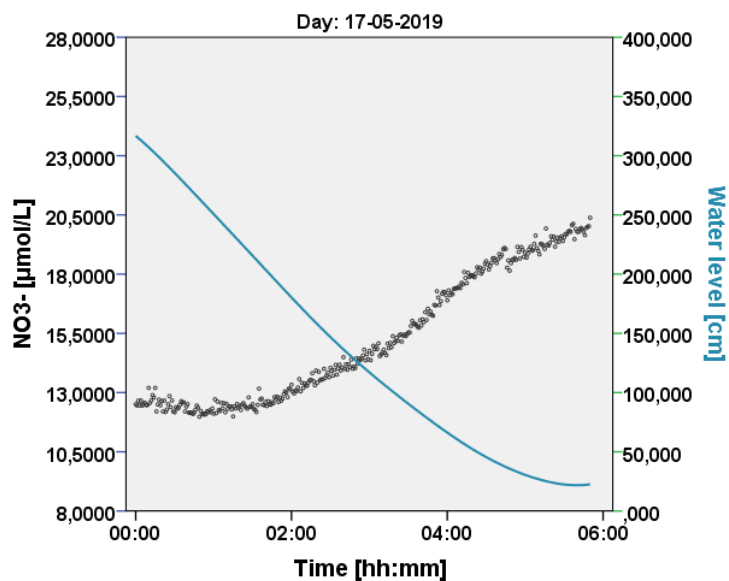


Figure 24. Variation in nitrate concentration across a tidal cycles measured on May 17th, 2019.

Table 4. Nitrate and water levels during high tides and low tides.

Date	Tidal intervall	NO3- [$\mu\text{mol/L}$]	Water level [cm]
15-May-2019	Low tide	18.6973	34.299
	High tide	19.8403	315.23
	Low tide	17.7878	57.302
	High tide	12.0362	339.753
16-May-2019	Low tide	18.7557	27.03
	High tide	25.403	326.006
	Low tide	19.244	47.009
	High tide	19.9291	345.791
17-May-2019	Low tide	19.794	21.798

4.1. Control variables

Pearson tests indicated significant negative correlations between nitrate concentrations and salinity, between nitrate and water temperature as well as between the water level and salinity, whilst a positive correlation between water temperature and salinity was revealed (as shown in table 5).

Table 5. Results of Pearson correlations testing the relationship between the control variables and NO_3^- concentration.

Variable 1		Variable 2			
		Water level	NO3-	Water temperature	Salinity
Water level	r		0.408	-0.016	-0.288
	p		< 0.001	0.531	< 0.001
	n		1484	1484	1484
NO3-	r	0.408		-0.210	-0.514
	p	< 0.001		< 0.001	< 0.001
	n	1484		1484	1484
Salinity	r	-0.288	-0.514	0.650	
	p	< 0.001	< 0.001	< 0.001	
	n	1484	1484	1484	

5. Discussion

Spatial and tide induced patterns of nitrate discharge in a beach ecosystem on Spiekeroog Island were examined during this study. Spatial patterns were researched by means of ex situ analyses of pore water samples, which were collected along ten transects, covering different segments of the littoral zone (HWL, runnel, ridge, LWL) and sampling depths (50cm and 100cm). Variability in nitrate levels across tidal cycles (temporal patterns) were in situ examined by deploying a spectral nitrate sensors at the Northern beach at the HWL and measuring for 60 hours.

5. 1. Temporal patterns

Examining nitrate concentration across tidal cycles indicated distinct temporal patterns. Patterns in nitrate differed greatly during falling and rising tides, which indicated a high impact of tides on nitrate fluctuations. During rising tides, nitrate concentration increased until a tidal level of approximately 15cm below the upcoming high tide level and then declined sharply during high tide resulting in moderate nitrate concentrations during high water. During falling tides, nitrate concentrations declined further until a tidal level of approximately 60 to 130cm below the previous high tide level. From this point on, nitrate concentration increased again until low tide. During and after low tide nitrate levels remained more stable but increased again until approximately 25cm below the water level of the upcoming high tide. During the first tidal cycle of each day, nitrate concentrations followed more stable curves, whilst during the second cycle of each day stronger fluctuations were observed. This pattern was observed across all examined tidal cycles and the curvilinear relationship between nitrate concentration and tidal level was revealed as statistical significant. At first glance, this pattern is unexpected due to outcomes of previous studies suggesting highest SGD rates during low tide, as a consequence of a steeper hydraulic gradient between pore and sea water during ebb tide, resulting in a more active flow of pore water into the sea (Billerbeck, 2005). However, besides the hydraulic gradient, variations in salinity and water temperature induced by fluctuating tidal levels might also contribute to the observed pattern in nitrate, since other studies found that the density gradient between pore water and sea water influences the intensity of SGD (Michael *et al.*, 2016).

Only a few field studies addressed the variability in nitrate transported by SGD across tidal cycles so far. However, a study conducted by Santos *et al.* (2009) examined variability of nitrate discharge across tidal cycles at a sandy beach in the Gulf of Mexico. Despite the differing study site and methodology of the research by Santos *et al.* (every 90 minutes a pore water sample was collected at the HWL at four different sampling stations across a time period of 16 hours and nitrate was measured ex situ using a standard colorimetric method) similar patterns were found: Shortly before high tide a peak in nitrate concentration was observed and during high tide nitrate levels decreased, whilst during low tide nitrate concentration increased until nitrate concentrations peaked again shortly before the next high water (Santos *et al.*, 2009). The study by Santos *et al.* (2009) concluded that the observed temporal pattern results from mixing of pore water and recirculating sea water during high water, which might also explain the observed temporal pattern in nitrate on Spiekeroog. Mixing of sea water and pore water during high tide might also explain the observed higher variability in nitrate concentrations during high tide compared to the more stable concentrations in nitrate during low tide.

A further explanation of the distinct temporal pattern might be the assumption of a time-delayed influx and exchange of pore water in the filter tube, resulting in time-delayed nitrate peaks. Time-delayed nitrate peaks as a result of time-delayed water exchange in the filter tubes might explain the contrary result of highest nitrate concentration shortly before high water and not during ebb tide as stated by Billerbeck (2005). The revealed negative correlation between salinity and water levels supports the assumption that a time-delayed water exchange in the filter tubes influenced the results of this study.

5.1.1. Limitations

Interference of very fine sediments causing reduced light availability presented a limitation in studying temporal patterns in nitrate. Whereas measurements conducted at the HWL were not affected, measurements conducted in the tidal runnel were interfered by fine sediments. Filter hoses, protecting the optical paths of the spectral sensors were used, however, mesh wide was likely too large (0.3 μ m). Therefore, it is recommended to consider the grain size in the choice of mesh wide in future studies. Apart from this, it should be mentioned that the day after finishing the tidal experiment full moon took place (on May 18, 2019) creating a spring tide, which let suggest that patterns in nitrate are less extreme during neap and average tides.

5.2. Spatial patterns

5.2.1 Cross-shore patterns

Distinct spatial patterns in nitrate were mainly revealed in the cross shore direction: A significant trend of increasing nitrate concentrations towards the higher shore was revealed, indicating highest nitrate concentration at the HWL, followed by samples collected at the ridge and in the runnel whilst samples collected at the LWL showed lowest nitrate concentrations. Samples collected at the HWL and at the LWL differed the most from each other and differed as well from sea water samples regarding nitrate concentrations. However, it needs to be noted, that the highest proportion of excluded samples was collected in the runnel (15 excluded samples were collected in the runnel, 10 samples at the LWL and 7 samples at the ridge) which might have affected the result. Previous research, found highest SGD rates in the runnel and at the LWL due to exfiltration and aggregation of pore water as a result of a steeper hydraulic gradient between the runnel/LWL and aquifers compared to the HWL/ridge (Scott *et al.*, 2011). Based on these previous studies, it was assumed that nitrate discharge follows similar patterns. A possible explanation for the observed pattern of increasing nitrate levels with increasing shore height might be the influence of oxygen. In general, nitrate and oxygen are positive correlated due to the nitrification of ammonium into nitrate under the influence of oxygen (Kaiser *et al.*, 2011). A positive correlation between nitrate and oxygen was also in this study revealed and the mean oxygen content in pore water at the HWL was found to be a multiple of the mean oxygen content in the runnel, at the ridge and LWL (as shown in appendix III), which might have affected cross-shore patterns found during this study. This suggestion is supported by outcomes of a study by Beck *et al.* (2017), which found higher nitrate concentrations higher at the shore, whereas closer to the LWL mostly ammonium were found.

Apart from this, highest variability in nitrate patterns in the cross-shore direction was observed in samples collected at the ridge and in the runnel, which is in line with a previous study by Waska *et al.* (2019a) investigating pore water chemistry at the Northern beach of Spiekeroog. The study by Waska *et al.* (2019a) concluded that high variability in pore water composition at the ridge and in the runnel is likely linked to extremers and faster morphological shifts in this segments of the littoral zone, as a result of high exposure to waves and tides.

5.2.2. Longshore patterns

In the longshore direction no significant trend in nitrate discharge was observed. However, the data showed diffuse discharge of nitrate and high longshore variability. This is in line with other research conducted at the Northern beach of Spiekeroog: The previous study by Waska *et al.* (2019a) suggests that diffuse patterns in nutrient discharge are likely linked to random factors. Consequently, the hypothesis of increasing nitrate levels towards the West, as a result of nutrient discharge from the tidal flats was not proven by this study.

5.2.3. Depth-dependent patterns

Analyses of depth-dependent differences in nitrate concentration did not show distinct patterns, but also high variability. Only in samples collected at the ridge, significant differences were observed which indicated higher nitrate concentrations in 50cm than in 100cm depth. Therefore, the hypothesis of increasing nitrate concentrations with depth due to lower salinity at greater depths (Rapaglia & Bokuniewicz, 2009) and the assumed negative correlation between NO_3^- and salinity (Knee *et al.*, 2010) was not proven by this study. However, due to limited sampling depths, it was not possible to investigate a possible trend in nitrate concentrations.

5.2.4. Limitations

Variability in nitrate concentrations across tidal levels was not considered during the collection of pore water samples to examine spatial patterns. However, results of the tidal experiment indicate that the tidal level effects nitrate concentration in pore water. The main proportion of pore water collected at the LWL was sampled during low tide and the majority of pore water collected at higher littoral zones was sampled at higher tidal levels (to extend the working time for sample collection). The analysis of temporal patterns revealed increasing nitrate levels at higher tidal levels (and a sharp decline shortly before high water) and the spatial analysis revealed much higher nitrate concentrations at the HWL compared to nitrate levels found in samples collected at the LWL, which let suggests that results of the spatial analysis are possibly influenced by the tidal level at the moment of sample collection. Therefore, it is highly recommended to consider the tidal level during sampling in future studies.

A further implication of studying spatial patterns in nitrate discharge, was the low sample size which resulted from excluding high numbers of samples due to nitrate levels under the detection limit ($< 1.0930 \mu\text{mol/L}$). A higher detection limit could be reached by increasing the sensor's optical path length, which requires larger quantities of pore water per sample (Pellerin *et al.*, 2013a) and therefore, it is recommended to increase pore water volume per sample in future studies.

Apart from this, it should be noted that the revealed negative correlations between nitrate and salinity as well as between nitrate and water temperature are commonly observed in science (Knee *et al.*, 2010) due to the dependence of the conductivity on the material and the resistance of the material (as a result of the capability to conduct electronic currents by ions serving as conductor), which in turn is linked to the temperature (McCleskey *et al.*, 2012). Therefore, the revealed negative correlations are rather an indicator for a correct measurement of salinity and temperature, than an interference of optical nitrate measurements (since salinity and temperature were considered during data preparation).

Eventually, the relatively low nitrate concentrations measured during this study at the Northern beach of Spiekeroog, support the findings of a study by Beck *et al.* (2017), which compared SGD rates on the Frisian barrier islands at sandy beaches facing the open North Sea and SGD rates at the back barrier tidal flats. The study concluded that SGD plays a key role in sandy beach systems as pathway for nutrients due to high permeability of sand, resulting in a higher volumes of pore water flowing into the sea compared to other sediment types (Beck *et al.*, 2017). However, on Spiekeroog, SGD from the backbarrier tidal flats is from greater importance for total nutrient budgets entering marine systems, due to the higher load of organic matter in the tidal flat system (Beck *et al.*, 2017). The Wadden Sea's tidal flats present a very unique ecosystem (Common Wadden Sea Secretariat, 2016) and in a global context, SGD in tidal flats is restricted to fewer areas and likely from minor importance as pathway for nutrients compared to SGD in sandy beach systems, which cover 31% of the Earth's shoreline (Luijendijk *et al.*, 2018).

6. Conclusion

SGD in sandy beach systems plays a significant role in transporting nitrate into marine waters, as shown in research before. Studying SGD as pathway for nitrate at the sandy beaches on Spiekeroog, revealed diffuse, but highly variable patterns in the longshore direction, whereas distinct patterns were found in the cross-shore direction and across tidal cycles. The relatively low nitrate concentrations found during this study support the findings of previous research suggesting a minor impact of SGD from the sandy beaches on Spiekeroog compared to SGD from the backbarrier tidal flats on total budgets of nitrogenous compounds entering the Southern North Sea. However, in other systems, where tidal flats are absent and impact of pollution by nitrogenous compounds is higher, SGD fluxes of nitrate from sandy beaches play likely a more important role.

Apart from this, the study further revealed the complexity of assessing SGD as pathway for nitrate and the large numbers of variables (tidal levels, salinity, water temperature, oxygen content and beach morphology) affecting the intensity and function of nitrate discharge. The variety of factors influencing SGD and side specific variability in these factors, impede the consideration of SGD as pathway for nitrate in current coastal management. However, this should not result in a negligence of SGD as pathway for nitrate but rather in assessing the magnitude of SGD in specific systems in order to enable the consideration of SGD as pathway for nitrate in coastal management. In areas where SGD has significant impact on nitrate budgets, monitoring and modelling of nitrate budgets should be adjusted in order to reduce the error rate in assessing nitrate budgets and the risk of eutrophication. Adjusted strategies for nitrate monitoring should be side specific and consider the tidal level and position (regarding the shore height) during monitoring. In addition, salinity, water temperature and oxygen concentration, which have significant impact on nitrate levels as shown in this study and various other studies should be considered in nitrate monitoring.

In conclusion, this study suggest to conduct further, system specific research investigating the magnitude and function of SGD as pathway for nitrate as well as the variability across tidal cycles and in the cross-shore direction. Incomplete knowledge about temporal and spatial variability in SGD as pathway for nitrate likely results in errors estimating nitrate budgets. Therefore, it is recommended to further examine the variability of nitrate discharge across tidal cycles and to conduct in situ measurements across longer periods. By measuring across longer time intervals, the observed pattern might be confirmed and nitrate levels during low tide and high tide, as well as water levels during nitrate peaks and lows statistically tested. Besides this, it is strongly recommended to examine the water exchange rate in the filter tubes in order to recalculate possible time-delayed nitrate peaks and lows. Also spatial patterns in nitrate should be further studied. Specifically, cross-shore patterns should be investigated by measuring ammonium concentration in addition to nitrate to examine whether the observed pattern of increasing nitrate levels with shore height is a result of higher oxygen concentrations at the higher shore causing nitrification of ammonium into nitrate. Apart from this, depth-depended patterns in nitrate discharge should be investigated by sampling more depth levels in order to find possible patterns, which might be linked to depth-depended variability in salinity, temperature and oxygen.

Conducting the recommended investigations and thereby reducing the remaining uncertainties regarding the magnitude of SGD as pathway of nitrate will likely contribute to the manageability of a complex component influencing the health of vulnerable and important ecosystems.

References

- Andersen, M. S. *et al.*, 2007. Discharge of nitrate-containing groundwater into a coastal marine environment. *Journal of Hydrology*, 336, pp. 98–114.
- Beck, M. & Brumsack, H.-J., 2012. Biogeochemical cycles in sediment and water column of the Wadden Sea: The example Spiekeroog Island in a regional context. *Ocean & Coastal Management*, 68, pp. 102-113.
- Beck, M. *et al.*, 2017. The drivers of biogeochemistry in beach ecosystems: A cross-shore transect from the dunes to the low-water line. *Marine Chemistry*, 190, pp. 35-50.
- Beusekom, J. E. van *et al.*, 2018. *Wadden Sea Quality Status Report - Eutrophication*. Wilhelmshaven: Common Wadden Sea Secretariat.
- Beusen, A. H. *et al.*, 2013. Global land–ocean linkage: direct inputs of nitrogen to coastal waters via submarine groundwater discharge. *Environmental Research Letters*, 8 (3), pp. 1-6.
- Billerbeck, M. (2005). *Pore water transport and microbial activity in intertidal Wadden Sea sediments*. Bremen: Universität Bremen.
- Bird, E. *et al.*, 2003. Coastal Geomorphology of Great Britain. [Graphic].
- Burnett, W. C. *et al.*, 2006. Quantifying submarine groundwater discharge in the coastal zone via multiple methods. *Science of the total Environment*, 367, pp. 498–543.
- Buss, S. *et al.*, 2005. *Attenuation of nitrate in the sub-surface environment*. Birmingham: Environment Agency.
- Campbell, N. *et al.*, 2014. *Biology a Global Approach (10th ed.)*. London: Pearson.
- Carl von Ossietzky Universität Oldenburg (2018). *BIME*. Retrieved on April 4, 2019, from <https://uol.de/en/icbm/collaborative-projects/bime/>
- Cho, H.-M. *et al.*, 2018. Radium tracing nutrient inputs through submarine groundwater discharge in the global ocean. *Scientific Reports*, 8. DOI: 10.1038/s41598-018-20806-2
- Common Wadden Sea Secretariat, 2016. *Report on the State of Conservation of the World Heritage property “The Wadden Sea (N1314)”*. Wilhelmshaven, Germany.
- Dijkema, K. S. (1991). Towards a habitat map of the Netherlands, German and Danish Wadden Sea. *Ocean & Shoreline Management*, 16, pp. 1-21.
- European Commission, 2016. *Press releases database*. Retrieved on June 10, 2019, from http://europa.eu/rapid/press-release_IP-16-1453_en.htm
- European Commission, 2018a. *Report from the commission to the council and the European parliament*. Brussels: European Commission.
- European Commission, 2018b. *Implementation of Council Directive 91/676/EEC concerning the protection of waters against pollution caused by nitrates from agricultural sources based on Member State reports for the period 2012–2015*. Brussels: European Commission.
- Herbert, R., 1999. Nitrogen cycling in coastal marine ecosystems. *FEMS Microbiology Reviews*, 23, pp. 563-590.

- Kaiser, M. *et al.*, 2011. *Marine ecology (2nd ed.)*. Oxford: Oxford University Press.
- Keppner, L. *et al.*, 2012. *Nitrates Report 2012*. Bonn: Federal Ministry for the Environment, Nature Conservation and Nuclear Safety (BMU).
- Knee, K. L. *et al.*, 2010. Nutrient inputs to the coastal ocean from submarine groundwater discharge in a groundwater-dominated system: Relation to land use (Kona coast, Hawaii, U.S.A.). *Limnology and Oceanography*, 55 (3), pp. 1105–1122.
- Kolbe, K. *et al.*, 1995. Macro algal mass development in the Wadden Sea: first experiences with a monitoring system. *Helgoländer Meeresuntersuchungen*, 49, pp. 519-528.
- Kwon, E. Y. *et al.*, 2014. Global estimate of submarine groundwater discharge based on an observationally constrained radium isotope mode. *Geophysical Research Letters*, 41 (23), pp. 8438-8444.
- Lecher, A. L., & Mackey, K. R., 2018. Synthesizing the Effects of Submarine Groundwater Discharge on Marine Biota. *Hydrology*, 5 (4), 60. DOI: 10.3390/hydrology5040060
- Lee, E. *et al.*, 2016. Periodic change in coastal microbial community structure associated with submarine groundwater discharge and tidal fluctuation. *Limnology & Oceanography*. DOI: 10.1002/lno.10433
- Luijendijk, A. *et al.*, 2018. The State of the World's Beaches. *Scientific Reports*, 8. DOI: 10.1038/s41598-018-24630-6.
- McCleskey, R. *et al.*, 2012. Comparison of electrical conductivity calculation methods for natural waters. *Limnology and Oceanography: Methods*, 10, pp. 952–967.
- McCoy, C.A. & Corbett, D.R., 2009. Review of submarine groundwater discharge (SGD) in coastal zones of the Southeast and Gulf Coast regions of the United States with management implications. *Journal of Environmental Management*, 90, pp. 644–651.
- Michael, A. *et al.*, 2016. Geologic influence on groundwater salinity drives large seawater circulation through the continental shelf: Geology drives seawater circulation. *Geophysical Research Letters*, 43 (20). DOI: 10.1002/2016GL070863.
- Michel, D. & Howa, H. L., 1999. Short-term morphodynamic response of a ridge and runnel system on a mesotidal sandy beach. *Journal of Coastal Research*, 15(2), pp. 428-437.
- Moore, W. S. (1996). Large groundwater inputs to coastal waters revealed by ²²⁶Ra enrichments. *Nature*, 380, pp. 612–614.
- Moosdorf, N. *et al.*, 2015. Submarine groundwater discharge from tropical islands: A review. *Grundwasser*, 20 (1), pp. 53-67.
- O'Neil, J. *et al.*, 2012. The rise of harmful cyanobacteria blooms: The potential roles of eutrophication and climate change. *Harmful Algae*, 14, pp. 313–334.
- OSPAR. (2010). *Quality Status Report 2010*. London: OSPAR Commission.
- Owen, T. (2000). *Grundlagen der modernen UV-Vis Spektroskopie - Ein Leitfaden*. Germany: Agilent Technologies.

- Pellerin, B. *et al.*, 2013a. *Optical Techniques for the Determination of Nitrate in Environmental Waters: Guidelines for Instrument Selection, Operation, Deployment, Maintenance, Quality Assurance, and Data Reporting*. Reston, Virginia: U.S.: Geological Survey.
- Pellerin, B. *et al.*, 2013b. *Optical Techniques for the Determination of Nitrate in Environmental Waters: Guidelines for Instrument Selection, Operation, Deployment, Maintenance, Quality Assurance, and Data Reporting*. Reston, Virginia: U.S.: Geological Survey. [Graphic].
- Pinet, P. (2013). *Invitation to oceanography (6th edition)*. Burlington: Jones & Bartlett Learning.
- Rapaglia, J. P., & Bokuniewicz, H. J. (2009). The effect of groundwater advection on salinity in pore waters of permeable sediments. *Limnology and Oceanography*, 54 (2), pp. 630–643.
- Röper, T. *et al.*, 2012. Groundwater ages, recharge conditions and hydrochemical evolution of a barrier island freshwater lens (Spiekeroog, Northern Germany). *Journal of Hydrology*, 454 (455), pp. 173-186.
- Röper, T. *et al.*, 2013. Freshwater lens formation below juvenile dunes on a barrier island (Spiekeroog, Northwest Germany). *Estuarine, Coastal and Shelf Science*, 121-122, pp.40-50.
- Santos, I. *et al.*, 2009. Tidal pumping drives nutrient and dissolved organic matter dynamics in a Gulf of Mexico subterranean estuary. *Geochimica et Cosmochimica Acta*, 73, pp. 1325–1339.
- Scott, T. *et al.*, 2011. Morphodynamic characteristics and classification of beaches in England and Wales. *Marine Geology*, 286, pp. 1-20.
- Stalker, J. C. *et al.*, 2009. Determining Spatial and Temporal Inputs of Freshwater, Including Submarine Groundwater Discharge, to a Subtropical Estuary Using Geochemical Tracers, Biscayne Bay, South Florida. *Estuaries and Coasts*, 32(4), pp. 694–708.
- Tamborski, J. *et al.*, 2017. Submarine groundwater discharge driven nitrogen fluxes to Long Island Sound, NY: Terrestrial vs. marine sources. *Geochimica et Cosmochimica Acta*, 218, pp. 40-57.
- Waska, H. *et al.*, 2019a. Spatial and Temporal Patterns of Pore Water Chemistry in the Inter-Tidal Zone of a High Energy Beach. *Frontiers in Marine Science*, 6 (154), pp. 1-16.
- Waska, H. *et al.*, 2019b. Spatial and Temporal Patterns of Pore Water Chemistry in the Inter-Tidal Zone of a High Energy Beach. *Frontiers in Marine Science*, 6 (154), pp. 1-16. [Graphic].
- Waska, H. *et al.*, 2019c. Spatial and Temporal Patterns of Pore Water Chemistry in the Inter-Tidal Zone of a High Energy Beach. *Frontiers in Marine Science*, 6 (154), pp. 1-16. [Graphic].
- Zielinski, O. *et al.*, 2011. Computation of nitrate concentrations in turbid coastal waters using an in situ ultraviolet spectrophotometer. *Journal of Sea Research*, 65 (4), pp. 456–460.

Appendix I

Measuring principles of the spectral sensor OPUS

The spectral sensor OPUS determines the concentration of a substance in an aquatic body by measuring its transmission (T) of light at a certain wavelength (nitrate at 210nm) (figure 1) and compares it with the transmission of ultra-pure water. By dividing the basic intensity of light through the current light intensity of the sample the transmission rate of the sample is calculated as following:

$$T = I/I_0$$

Due to the linear relationship between the absorption (which is a logarithmic function of the transmission) and concentration, the absorption is commonly used instead of the transmission rate:

$$A = -\log T$$

(Owen, 2000)

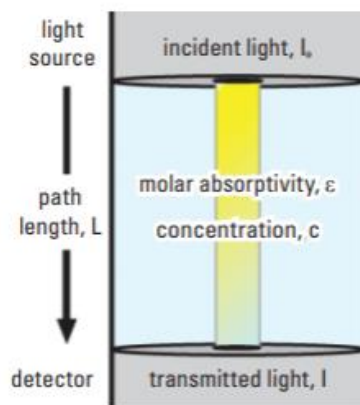


Figure 1. General measuring principle of photometers (Pellerin, et al., 2013b).

Where

T is the transmission rate (%)

I is the current light intensity of the sample

I_0 is the basic intensity of light (usually of ultra-pure water)

A is the Absorption

Appendix II
Equipment



Figure 2. Waterproof subcon-M8 adapters constructed for the tidal experiment.



Figure 3. The spectral sensor OPUS deep sea with a self-constructed optical path protector grid.

Appendix III

Model assumptions – Spatial patterns

Table 1. Results of normality and variance tests per segment of the littoral zone.

Variable	Group	Test	df	D	p	
NO ₃ -	Sea water	Shapiro-Wilk	8	0.991	0.996	
NO ₃ -	HWL	Shapiro-Wilk	17	0.940	0.316	
NO ₃ -	Runnel	Shapiro-Wilk	3	0.834	0.199	
NO ₃ -	Ridge	Shapiro-Wilk	11	0.906	0.217	
NO ₃ -	LWL	Shapiro-Wilk	7	0.772	0.021	
lg10 NO ₃ -	Sea water	Shapiro-Wilk	8	0.995	1.000	
lg10 NO ₃ -	HWL	Shapiro-Wilk	17	0.959	0.613	
lg10 NO ₃ -	Runnel	Shapiro-Wilk	3	0.947	0.558	
lg10 NO ₃ -	Ridge	Shapiro-Wilk	11	0.870	0.077	
lg10 NO ₃ -	LWL	Shapiro-Wilk	7	0.814	0.057	
Variable	Groups	Test	df1	df2	F	p
NO ₃ -	HWL, ridge, LWL, sea water	Leven's test	3	40	14.966	< 0.001
lg10 NO ₃ -	HWL, ridge, LWL, sea water	Leven's test	3	40	24.632	< 0.001

Table 2. Results of normality and variance tests per segment of the littoral zone and depth level.

Variable	Group		Test	df	D	p	
	Depth level [cm]	Segment littoral zone					
NO ₃ -	50	HWL	Shapiro-Wilk	8	0.943	0.642	
NO ₃ -	100	HWL	Shapiro-Wilk	9	0.915	0.352	
NO ₃ -	50	Runnel	Shapiro-Wilk	3	0.834	0.199	
NO ₃ -	50	Ridge	Shapiro-Wilk	7	0.950	0.731	
NO ₃ -	100	Ridge	Shapiro-Wilk	4	0.655	0.003	
NO ₃ -	50	LWL	Shapiro-Wilk	3	0.856	0.258	
NO ₃ -	100	LWL	Shapiro-Wilk	4	0.769	0.057	
lg10 NO ₃ -	50	HWL	Shapiro-Wilk	8	0.934	0.555	
lg10 NO ₃ -	100	HWL	Shapiro-Wilk	9	0.924	0.429	
lg10 NO ₃ -	50	Runnel	Shapiro-Wilk	3	0.947	0.558	
lg10 NO ₃ -	50	Ridge	Shapiro-Wilk	7	0.914	0.425	
lg10 NO ₃ -	100	Ridge	Shapiro-Wilk	4	0.746	0.056	
lg10 NO ₃ -	50	LWL	Shapiro-Wilk	3	0.900	0.385	
lg10 NO ₃ -	100	LWL	Shapiro-Wilk	4	0.814	0.13	
Variable	Groups		Test	df1	df2	F	p
	Depth level [cm]	Segment littoral zone					
NO ₃ -	50, 100	HWL	Leven's test	1	15	3.016	0.103
NO ₃ -	50, 100	Ridge	Leven's test	1	9	0.814	0.390
lg10 NO ₃ -	50, 100	HWL	Leven's test	1	15	1.341	0.265
lg10 NO ₃ -	50, 100	Ridge	Leven's test	1	9	1.506	0.251

Table 3. Results of normality tests for the variable NO₃- concentration.

Variable	Test	df	D	p
NO ₃ -	Shapiro-Wilk	44	0.823	< 0.001
lg10 NO ₃ -	Shapiro-Wilk	44	0.927	0.008

Control variables – Spatial patterns

Table 4. Mean values of the control variables per segment of the littoral zone and in sea water samples.

Littoral zone	HWL	Runnel	Ridge	LWL	Sea water
n	17	18	18	17	8
\bar{x} salinity [PSU]	25.6996	27.1819	26.1211	29.1721	23.5413
SD	3.0571	4.1933	3.9688	6.1812	5.3978
\bar{x} water temperature [C°]	8.0941	8.6167	8.1778	8.1529	7.5625
SD	0.7462	0.6355	0.7175	0.4110	0.4241
O2 content [%]	76.9177	4.2401	22.6729	3.7116	97.6975
SD	27.5693	3.4818	32.6975	2.7080	0.4175

Table 5. Results of normality tests for the control variables.

Variable	Test	df	D	p
Salinity [PSU]	Shapiro-Wilk	38	0.98	0.715
Water temperature [C°]	Shapiro-Wilk	38	0.964	0.25
O2 content [%]	Shapiro-Wilk	38	0.799	< 0.001
lg10 of salinity	Shapiro-Wilk	38	0.981	0.738
lg10 of water temperature	Shapiro-Wilk	38	0.97	0.42
lg10 of O2 content	Shapiro-Wilk	38	0.845	< 0.001
Square root of salinity	Shapiro-Wilk	38	0.982	0.773
Square root of water temperature	Shapiro-Wilk	38	0.968	0.339
Square root of O2 content	Shapiro-Wilk	46	0.827	< 0.001

Table 6. Results of Spearman correlations testing the relationship between the control variables and NO₃⁻ concentration. The results indicate, that model assumption of a multiple regression are not satisfy.

Variable 1		Variable 2			
		Salinity	O2 content	NO ₃ ⁻	Water temperature
Water temperature	ρ	-0.166	0.108	0.034	
	p	0.32	0.519	0.841	
	n	38	38	38	
Salinity	ρ		-0.696	-0.39	0.152
	p		< 0.001	0.009	0.325
	n		38	38	38
O2 content	ρ	-0.696		0.682	-0.177
	p	< 0.001		< 0.001	0.251
	n	38		38	38
NO ₃ ⁻	ρ	-0.602	0.504		0.05
	p	< 0.001	< 0.001		0.749
	n	38	38		38

Appendix IV

Model assumptions – Temporal patterns

Table 7. Results of normality tests (NO_3^- concentration during rising tides).

Variable	Test	df	D	p
NO_3^-	Kolmogorov-Smirnov	1484	0.075	< 0.001
lg10 NO_3^-	Kolmogorov-Smirnov	1484	0.085	< 0.001
Square root of NO_3^-	Kolmogorov-Smirnov	1484	0.078	< 0.001

Table 8. Results of normality tests (NO_3^- concentration during falling tides).

Variable	Test	df	D	p
NO_3^-	Kolmogorov-Smirnov	1747	0.05	< 0.001
lg10 NO_3^-	Kolmogorov-Smirnov	1747	0.075	< 0.001
Square root of NO_3^-	Kolmogorov-Smirnov	1747	0.059	< 0.001

Table 9. Results of normality tests (control variables during rising tides).

Variable	Test	df	D	p
Salinity [PSU]	Kolmogorov-Smirnov	1484	0.314	< 0.001
Water level [cm]	Kolmogorov-Smirnov	1484	0.089	< 0.001
Water temperature [C°]	Kolmogorov-Smirnov	1484	0.100	< 0.001
lg10 of salinity	Kolmogorov-Smirnov	1484	0.320	< 0.001
lg10 of water level	Kolmogorov-Smirnov	1484	0.154	< 0.001
lg10 of water temperature	Kolmogorov-Smirnov	1484	0.091	< 0.001
Square root of salinity	Kolmogorov-Smirnov	1484	0.316	< 0.001
Square root of water level	Kolmogorov-Smirnov	1484	0.116	< 0.001
Square root of water temperature	Kolmogorov-Smirnov	1484	0.096	< 0.001

Table 10. Results of normality tests (control variables during falling tides).

Variable	Test	df	D	p
Salinity [PSU]	Kolmogorov-Smirnov	1747	0.319	< 0.001
Water level [cm]	Kolmogorov-Smirnov	1747	0.094	< 0.001
Water temperature [C°]	Kolmogorov-Smirnov	1747	0.082	< 0.001
lg10 of salinity	Kolmogorov-Smirnov	1747	0.324	< 0.001
lg10 of water level	Kolmogorov-Smirnov	1747	0.094	< 0.001
lg10 of water temperature	Kolmogorov-Smirnov	1747	0.082	< 0.001
Square root of salinity	Kolmogorov-Smirnov	1747	0.322	< 0.001
Square root of water level	Kolmogorov-Smirnov	1747	0.076	< 0.001
Square root of water temperature	Kolmogorov-Smirnov	1747	0.082	< 0.001

Table 11. Results of normality tests indicating normal distribution of nitrate concentrations during high and low tide.

Tidal level	Test	df	D	p
High water	Shapiro-Wilk	4	0.933	0.615
Low water	Shapiro-Wilk	5	0.973	0.895

Table 12. Water levels during peaks and low points in NO₃⁻ concentration per tidal cycle.

Date	Extreme value	Tidal cycle of the day	NO ₃ ⁻ [μmol/L]	Water level [cm]
15-May-2019	Peak	1st	23.712	300.516
	Low point	1st	14.7463	223.849
	Peak	2nd	21.3714	313.296
	Low point	2nd	8.9394	279.487
16-May-2019	Peak	1st	25.4816	310.945
	Low point	1st	9.6281	212.04
	Peak	2nd	26.1098	320.018
	Low point	2nd	13.8589	219.194

Control variables – Temporal patterns

Table 13. Mean salinity and water temperature during rising and falling tides.

Tidal level	Rising tides	Falling tides
n	1484	1747
\bar{x} salinity [PSU]	29.2758	29.9328
SD	4.7025	4.04344
\bar{x} water temperature [C°]	11.8228	12.2561
SD	0.53199	0.78185

Table 14. Results of Pearson correlations testing the relationship between the control variables and NO₃⁻ concentration (during rising tides). The results indicate, that model assumption of a multiple regression are not satisfy.

Variable 1		Variable 2			
		Water level	NO ₃ ⁻	Water temperature	Salinity
Water level	r		0.408	-0.016	-0.288
	p		< 0.001	0.531	< 0.001
	n		1484	1484	1484
NO ₃ ⁻	r	0.408		-0.210	-0.514
	p	< 0.001		< 0.001	< 0.001
	n	1484		1484	1484
Salinity	r	-0.288	-0.514	0.650	
	p	< 0.001	< 0.001	< 0.001	
	n	1484	1484	1484	

Table 15. Results of Pearson correlations testing the relationship between the control variables and NO₃⁻ concentration (during falling tides). The results indicate, that model assumption of a multiple regression are not satisfy.

Variable 1		Variable 2			
		Water level	NO ₃ ⁻	Water temperature	Salinity
Water level	r		-0.465	0.012	-0.225
	p		< 0.001	0.624	< 0.001
	n		1747	1747	1747
NO ₃ ⁻	r	-0.465		-0.442	-0.465
	p	< 0.001		< 0.001	< 0.001
	n	1747		1747	1747
Salinity	r	-0.225	-0.465	0.656	
	p	< 0.001	< 0.001	< 0.001	
	n	1747	1747	1747	

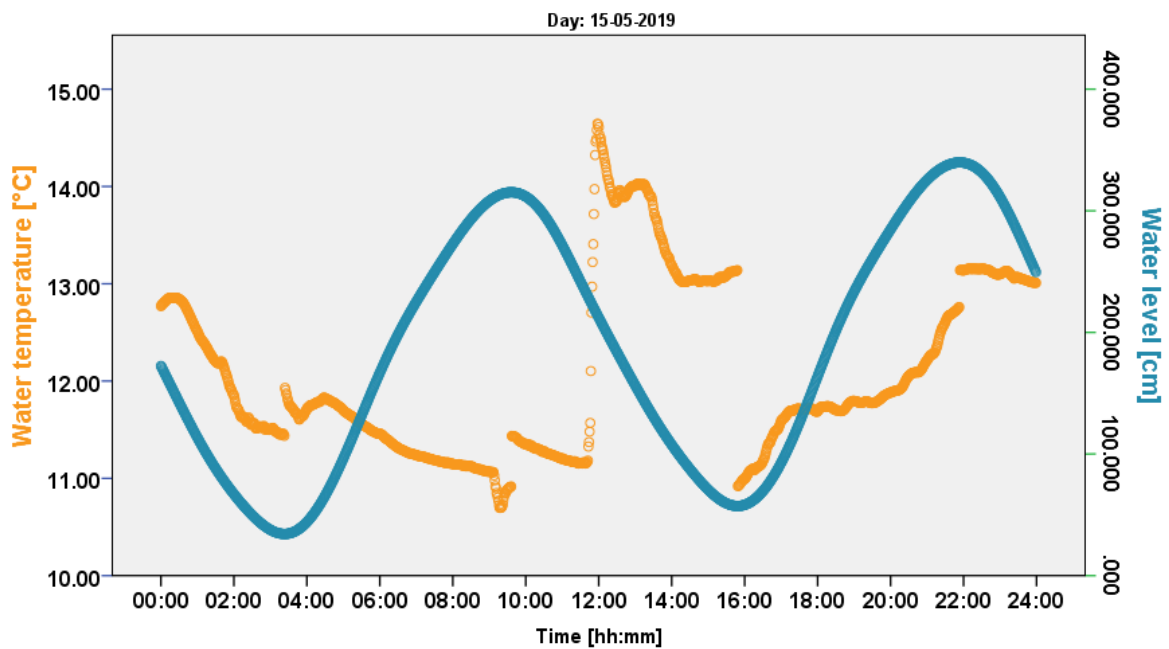


Figure 4. Variation in water temperature across two tidal cycles measured on May 15th, 2019.

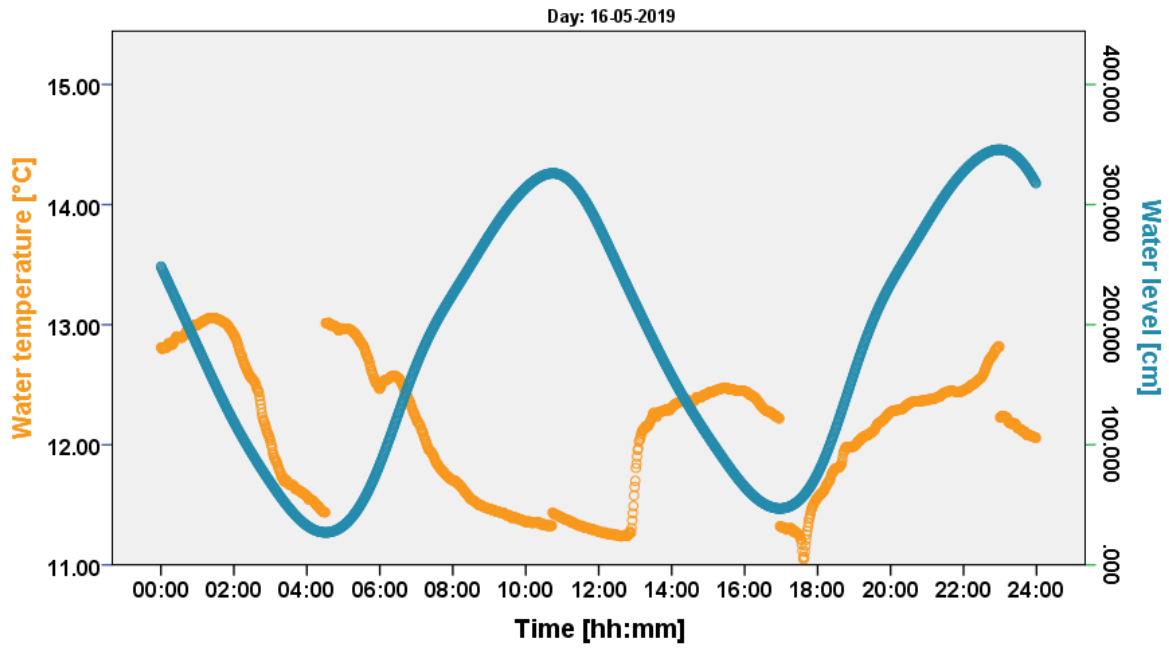


Figure 5. Variation in water temperature across two tidal cycles measured on May 16th, 2019.

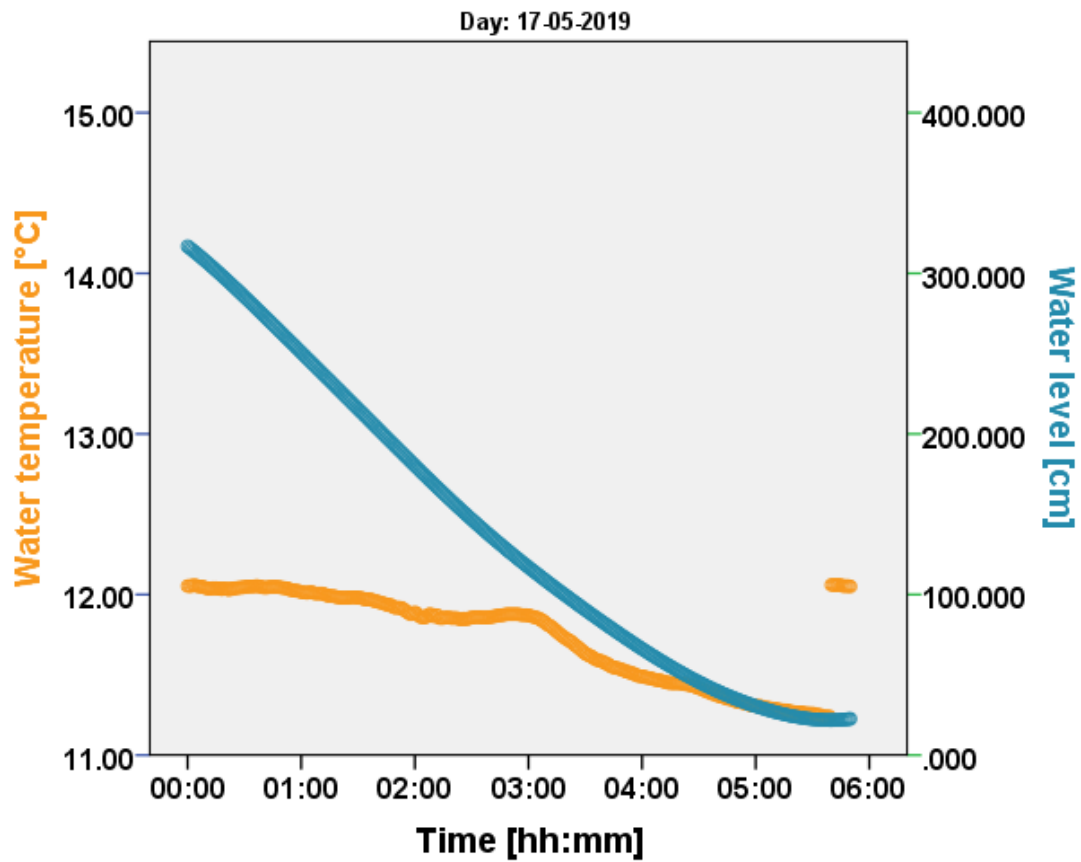


Figure 6. Variation in water temperature across 6 hours measured on May 17th, 2019.

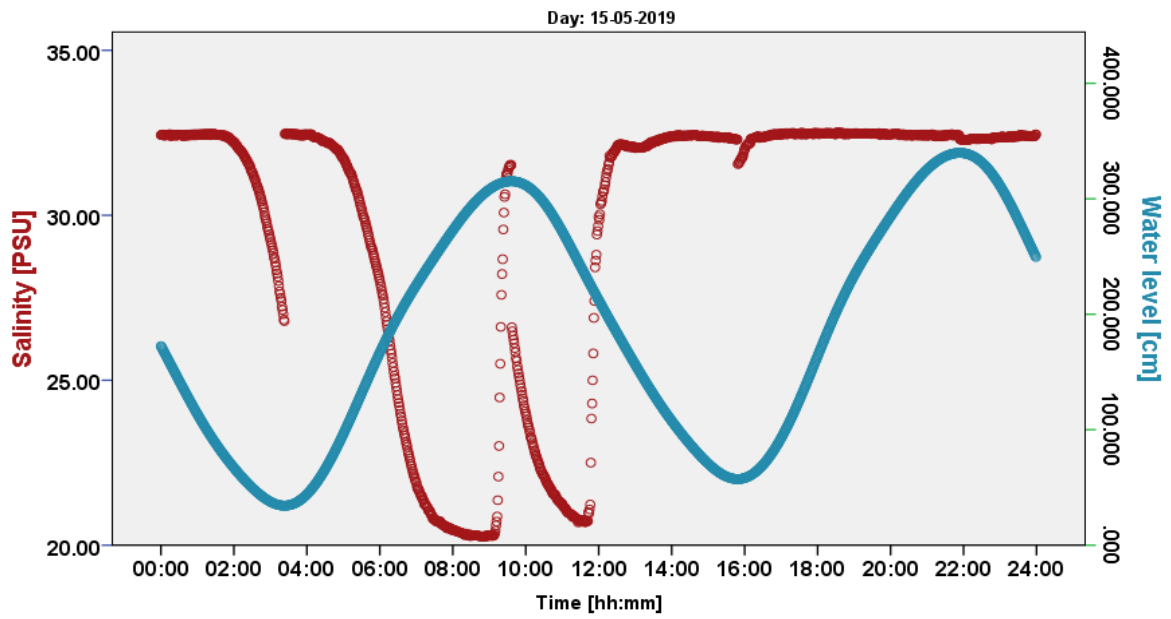


Figure 7. Variation in salinity across two tidal cycles measured on May 15th, 2019.

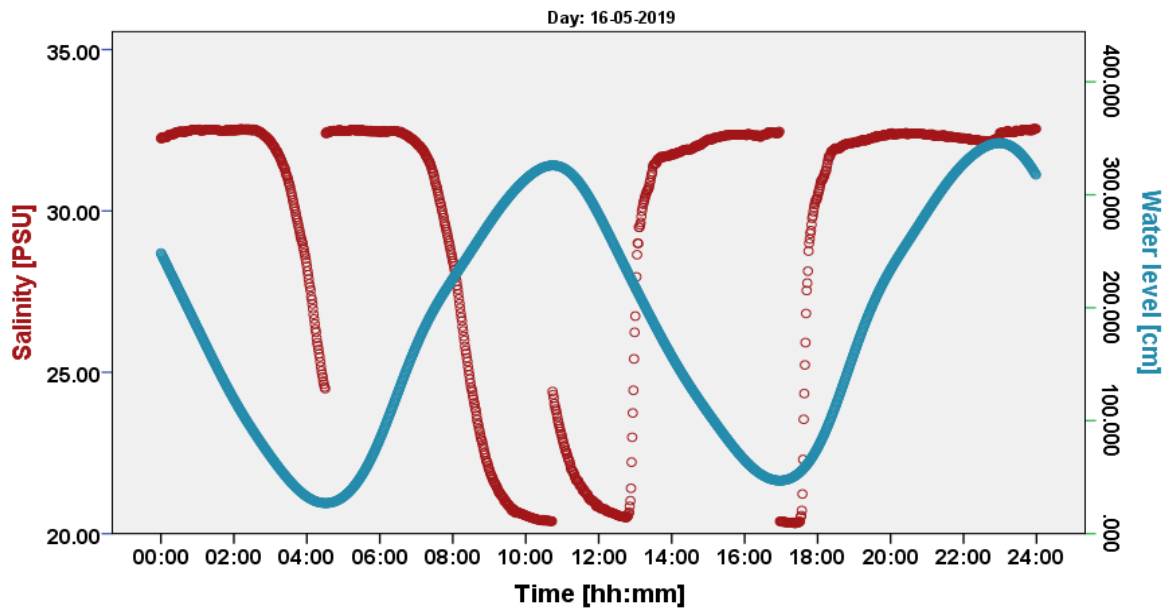


Figure 8. Variation in salinity across two tidal cycles measured on May 16th, 2019.

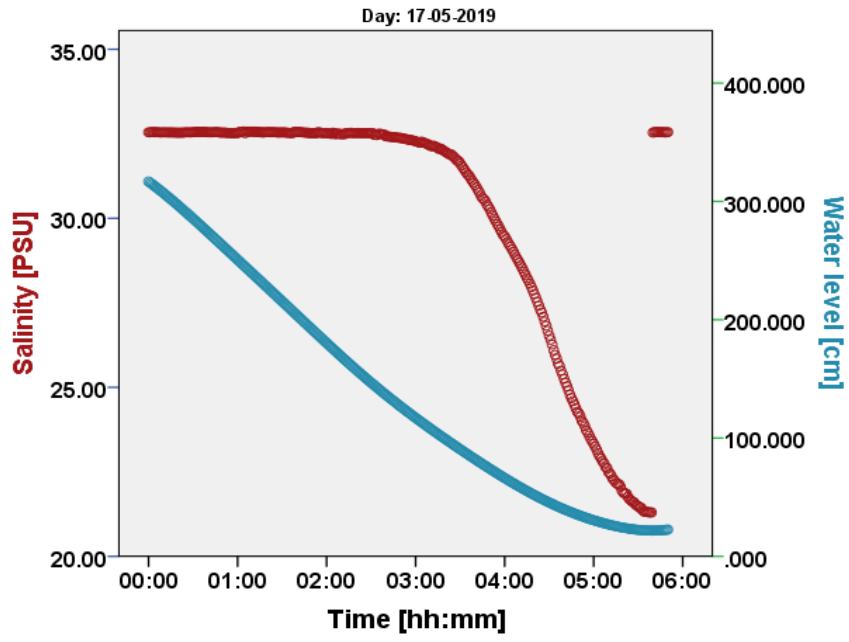


Figure 9. Variation in salinity across 6 hours measured on May 17th, 2019.

Appendix V

GPS coordinates

Table 16. GPS coordinates of the sampling points.

Sampling point	Transect no	Littoral zone	UTM coordinates*	
			x	y
44	Sea water	Sea water	413881	5960093
85	Sea water	Sea water	412740	5959396
A19	Sea water	Sea water	414775	5960102
8	1	Runnel	415113	5960033
19	1	HWL	415076	5959890
20	1	HWL	415076	5959890
25	1	LWL	415141	5960167
26	1	Ridge	415110	5960056
27	1	Runnel	415113	5960033
31	1	LWL	415141	5960167
32	1	Ridge	415110	5960056
A1	2	HWL	414781	5959916
A14	2	LWL	414775	5960102
A17	2	Runnel	414780	5960003
A18	2	LWL	414775	5960102
A2	2	Ridge	414778	5960040
A5	2	Runnel	414780	5960003
A6	2	HWL	414781	5959916
A9	2	Ridge	414778	5960040
14	3	LWL	414459	5960036
A11	3	Runnel	414472	5959948
A12	3	Runnel	414472	5959948
A16	3	HWL	414475	5959909
A20	3	HWL	414475	5959909
A3	3	Ridge	414468	5959987
A4	3	LWL	414459	5960036
A8	3	Ridge	414468	5959987
17	4	Ridge	414192	5959934
18	4	Runnel	414191	5959908
24	4	Runnel	414191	5959908
34	4	LWL	414201	5959990
35	4	HWL	414191	5959848
42	4	HWL	414191	5959848
47	4	Ridge	414192	5959934
2	5	Ridge	413955	5959898
7	5	Runnel	413877	5959846
9	5	LWL	413881	5960083
28	5	Ridge	413955	5959898

37	5	LWL	413881	5960083
43	5	HWL	413883	5959829
45	5	HWL	413883	5959829
50	5	Runnel	413877	5959846
23	6	Runnel	413612	5959680
29	6	Ridge	413581	5959734
30	6	LWL	413477	5959949
36	6	HWL	413624	5959666
48	6	Runnel	413612	5959680
76	6	LWL	413477	5959949
92	6	Ridge	413581	5959734
15	7	Ridge	413302	5959604
21	7	LWL	413184	5959812
38	7	LWL	413184	5959812
40	7	HWL	413371	5959489
49	7	Ridge	413302	5959604
75	7	HWL	413371	5959489
78	7	Runnel	413355	5959508
86	7	Runnel	413355	5959508
51	8	Runnel0	413081	5959323
52	8	Runnel	413093	5959354
53	8	Ridge	413052	5959426
54	8	Runnel	413093	5959354
57	8	LWL	412892	5959602
63	8	Ridge	413052	5959426
64	8	HWL	413145	5959298
65	8	HWL	413145	5959298
82	8	LWL	412892	5959602
46	9	HWL	412930	5959088
66	9	LWL	412640	5959386
73	9	Ridge	412761	5959258
74	9	Ridge	412761	5959258
77	9	Runnel	412889	5959131
81	9	LWL	412640	5959386
84	9	Runnel	412889	5959131
87	9	HWL	412930	5959088
* Coordinate system = WGS84 N32				

Table 17. GPS coordinates of the in situ deployed nitrate sensors.

Sensor location	UTM coordinates*	
	x	y
Runnel	415181	5959992
HWL	415166	5959992
* Coordinate system = WGS84 N32		

Appendix VI

Summary of excluded samples

Table 18. Excluded samples due to nitrate concentrations under the detection limit

Sampling point	Transect no	Segment littoral zone	Sampling depth [cm]
27	1	Runnel	100
A17	2	Runnel	100
A12	3	Runnel	100
7	5	Runnel	100
24	4	Runnel	100
23	6	Runnel	100
86	7	Runnel	100
A5	2	Runnel	50
A11	3	Runnel	50
78	7	Runnel	50
18	4	Runnel	50
77	9	Runnel	100
54	8	Runnel	50
84	9	Runnel	50
52	8	Runnel	100
A9	2	Ridge	100
49	7	Ridge	100
47	4	Ridge	100
29	6	Ridge	100
2	5	Ridge	100
A2	2	Ridge	50
17	4	Ridge	50
A18	2	LWL	100
38	7	LWL	100
37	5	LWL	100
34	4	LWL	100
A14	2	LWL	50
14	3	LWL	50
31	1	LWL	50
9	5	LWL	50
30	6	LWL	50
81	9	LWL	100